



American Society of Hematology  
2021 L Street NW, Suite 900,  
Washington, DC 20036  
Phone: 202-776-0544 | Fax 202-776-0545  
editorial@hematology.org

## Endothelial-leukemia interactions remodel drug responses uncovering T-ALL vulnerabilities

Tracking no: BLD-2022-015414R1

Luca Vincenzo Cappelli (Hematology, Department of Translational and Precision Medicine, Sapienza University, Italy) Danilo Fiore (Department of Molecular Medicine and Medical Biotechnology, University of Naples Federico II, 80131 Naples, Italy, Italy) Jude Phillip (Weill Cornell Medicine, United States) Liron Yoffe (Institute for Computational Biomedicine & Caryl and Israel Englander Institute for Precision Medicine, Weill Cornell Medicine, United States) Filomena Di Giacomo (Sapienza University, ) William Chiu (Weill Cornell Medicine, United States) Yang Hu (Weill Cornell Medical College, United States) Clarisse Kayembe (Weill Cornell Medicine, United States) Michael Ginsberg (Angiocrine Bioscience, ) Lorena Consolino (University of Turin, Italy) Jose Gabriel Barcia Duran (Weill Cornell Medicine, United States) Nahuel Zamponi (Weill Cornell Medicine, United States) Ari Melnick (Weill Cornell Medical College, Cornell University, United States) Francesco Boccalatte (NYU School of Medicine, United States) Wayne Tam (Weill Cornell Medicine, United States) Olivier Elemento (Weill Cornell Medical College, United States) Sabina Chiaretti (Hematology, Department of Translational and Precision Medicine, Sapienza University, Italy) Anna Guarini (SAPIENZA UNIVERSITY, Italy) Robin Foà (Hematology, Sapienza University of Rome, Italy) Leandro Cerchietti (Weill Cornell Medical College, United States) Shahin Rafii (Weill Cornell Medicine, United States) Giorgio Inghirami (Weill Cornell Medicine, United States)

### Abstract:

T-cell acute lymphoblastic leukemia (T-ALL) is an aggressive and often incurable disease. To uncover therapeutic vulnerabilities, we first developed T-ALL patient-derived tumor-xenografts (PDX) and exposed PDX cells to a library of 433 clinical-stage compounds *in vitro*. We identified 39 broadly active compounds with anti-leukemia activity.

Since endothelial cells (ECs) can alter drug responses in T-ALL, we developed an endothelial cells (ECs) / T-ALL co-culture system. We found that ECs provide pro-tumorigenic signals and mitigate drug responses to individual T-ALL PDX. ECs broadly rescued several compounds in most of the models, while other drugs were rescued only in individual PDXs suggesting unique crosstalk interactions and/or intrinsic tumor features.

Mechanistically, co-cultured T-ALL and ECs underwent bi-directional transcriptomic changes at the single-cell level, highlighting distinct “education signatures”. These changes were linked to a bi-directional regulation of multiple pathways in T-ALL and ECs. Remarkably, *in-vitro* EC-educated T-ALL cells mirrored *ex-vivo* splenic T-ALL at the single-cell resolution. Lastly, five effective drugs from the two drug screenings were tested *in vivo* and shown to effectively delay tumor growth/dissemination and prolonging the overall survival (OS). We anticipate that this T-ALL-EC platform can contribute to elucidating leukemia-microenvironment interactions and identify effective compounds and therapeutic vulnerabilities.

**Conflict of interest:** COI declared - see note

**COI notes:** Michael Ginsberg is currently employed at Angiocrine Bioscience, San Diego, CA, USA. The other authors declare no potential conflicts of interest. Shahin Rafii is a co-founder and non-paid consultant to Angiocrine Biosciences, San Diego, CA, USA.

**Preprint server:** No;

**Author contributions and disclosures:** L. V. Cappelli: Conceptualization, formal analysis, methodology, writing-original draft, writing-review and editing. D. Fiore: Conceptualization, formal analysis, methodology, writing-original draft, writing-review and editing. J.M. Phillip: Conceptualization, formal analysis, methodology, writing-original draft, writing-review and editing. L. Yoffe: Conceptualization, formal analysis, methodology, writing-original draft, writing-review and editing. F. Di Giacomo: Conceptualization, formal analysis, methodology, writing-original draft, writing-review and editing. Y. Hu: Formal analysis, methodology, editing. C. Kayembe: Formal analysis, methodology, editing. W. Chiu: Formal analysis, methodology. M. Ginsberg: Conceptualization, formal analysis, methodology, editing. L. Consolino: Conceptualization, formal analysis, methodology, editing. J.G.B Duran: Conceptualization, methodology, editing. N. Zamponi: Conceptualization, formal analysis, methodology, editing. A.M. Melnick: Conceptualization, writing-review and editing. W. Tam: Conceptualization, formal analysis, methodology, writing-original draft, writing-review and editing. O. Elemento: Conceptualization, formal analysis, writing-review and editing. S. Chiaretti: Conceptualization, writing-review and editing. A. Guarini: Conceptualization, writing-review and editing. R. Foa: Conceptualization, writing-review and editing. L. Cerchietti: Conceptualization, formal analysis, methodology, writing-original draft, writing-review and editing. S. Rafii: Conceptualization, formal analysis, methodology, writing-original draft, writing-review and editing. G. Inghirami: Conceptualization, data curation, formal analysis, supervision, methodology, writing-original draft, project administration, writing-review and editing.

**Non-author contributions and disclosures:** No;

**Agreement to Share Publication-Related Data and Data Sharing Statement:** Data including RNA sequencing may be found in a data supplement available with the online version of this article.

**Clinical trial registration information (if any):**

1   **Endothelial-leukemia interactions remodel drug responses uncovering T-**  
2   **ALL vulnerabilities**

3

4   Luca Vincenzo Cappelli<sup>1,2</sup>, Danilo Fiore<sup>1,3,4</sup>, Jude M. Phillip<sup>5</sup>, Liron Yoffe<sup>1,6</sup>,  
5   Filomena Di Giacomo<sup>1</sup>, William Chiu<sup>1</sup>, Yang Hu<sup>6</sup>, Clarisse Kayembe<sup>1</sup>, Michael  
6   Ginsberg<sup>7</sup>, Lorena Consolino<sup>8</sup>, Jose Gabriel Barcia Duran<sup>9</sup>, Nahuel Zamponi<sup>10</sup>, Ari  
7   Melnick<sup>10</sup>, Francesco Boccalatte<sup>11</sup>, Wayne Tam<sup>1</sup>, Olivier Elemento<sup>6</sup>, Sabina  
8   Chiaretti<sup>2</sup>, Anna Guarini<sup>2</sup>, Robin Foà<sup>2</sup>, Leandro Cerchietti<sup>10\*</sup>, Shahin Rafii<sup>9\*</sup>,  
9   Giorgio Inghirami<sup>1,12\*</sup>

10

11   1. Department of Pathology and Laboratory Medicine, Weill Cornell Medicine,  
12   10065, New York, NY, USA

13   2. Department of Translational and Precision Medicine, Sapienza University of  
14   Rome, 00161 Rome, Italy

15   3. Department of Molecular Medicine and Medical Biotechnology, University of  
16   Naples Federico II, 80131 Naples, Italy

17   4. Institute for Experimental Endocrinology and Oncology, "G. Salvatore" IEOS,  
18   Consiglio Nazionale delle Ricerche (CNR), 80131 Naples, Italy.

19   5. Departments of Biomedical Engineering, Chemical and Biomolecular  
20   Engineering, Oncology, Johns Hopkins University, Baltimore, MD, USA

21   6. Institute for Computational Biomedicine & Caryl and Israel Englander Institute  
22   for Precision Medicine, Weill Cornell Medicine, 10021, New York, NY, USA  
23   USA

24   7. Angiocrine Bioscience, 92122, San Diego CA, USA

25   8. Department of Molecular Biotechnology and Health Sciences, University of  
26   Turin, 10126, Turin, Italy

27   9. Department of Medicine, Ansary Stem Cell Institute, Division of Regenerative  
28   Medicine, Weill Cornell Medicine, 10065, New York, NY,

29   10. Department of Medicine, Hematology and Oncology Division, Weill Cornell  
30   Medicine and the New York Presbyterian Hospital, 10065, New York, NY, USA.

31   11. Department of Pathology, New York University School of Medicine, New York,  
32   NY, USA

33   12. Lead Contact

34

35   Running Title: Endothelial-leukemia interactions in T-ALL

36

37   Keywords: T-ALL; PDX; Endothelial cells; Drug discovery; Precision medicine

38

39

40

41   **Note:** L.V. Cappelli, D. Fiore, J.M. Phillip, L. Yoffe and F. Di Giacomo contributed  
42   equally to this article.

43

1      **Correspondent Authors:**

2  
3      Giorgio Inghirami, M.D.  
4      E-mail: ggi9001@med.cornell.edu

5  
6      Shahin Rafii, M.D.  
7      E-mail: sraffi@med.cornell.edu.

8  
9      Leandro Cerchietti, M.D.  
10     E-mail: lec2010@med.cornell.edu

11  
12     **Lead Contact:**

13     Giorgio Inghirami, M.D.  
14     E-mail: ggi9001@med.cornell.edu

15  
16  
17     Presented as oral abstract at the 63rd annual meeting of the American Society of  
18     Hematology, Atlanta, GA, December 2021. Abstract #704.

1   **Key Points**

2

- 3   • We generated 22 T-ALL PDX models to identify T-ALL liabilities and  
4   investigate the interplay between leukemia and endothelial cells.
- 5   • We identified active compounds, some of which were effective in-vivo.  
6   Interacting EC and T-ALL underwent reciprocal transcriptomic changes.

1   **Abstract**

2   T-cell acute lymphoblastic leukemia (T-ALL) is an aggressive and often incurable  
3   disease. To uncover therapeutic vulnerabilities, we first developed T-ALL patient-  
4   derived tumor-xenografts (PDX) and exposed PDX cells to a library of 433 clinical-  
5   stage compounds *in vitro*. We identified 39 broadly active compounds with anti-  
6   leukemia activity.

7   Since endothelial cells (ECs) can alter drug responses in T-ALL, we developed an  
8   endothelial cells (ECs) / T-ALL co-culture system. We found that ECs provide pro-  
9   tumorigenic signals and mitigate drug responses to individual T-ALL PDX. ECs  
10   broadly rescued several compounds in most of the models, while other drugs  
11   were rescued only in individual PDXs suggesting unique crosstalk interactions  
12   and/or intrinsic tumor features.

13   Mechanistically, co-cultured T-ALL and ECs underwent bi-directional  
14   transcriptomic changes at the single-cell level, highlighting distinct “education  
15   signatures”. These changes were linked to a bi-directional regulation of multiple  
16   pathways in T-ALL and ECs. Remarkably, *in-vitro* EC-educated T-ALL cells  
17   mirrored *ex-vivo* splenic T-ALL at the single-cell resolution. Lastly, five effective  
18   drugs from the two drug screenings were tested *in vivo* and shown to effectively  
19   delay tumor growth/dissemination and prolonging the overall survival (OS). We  
20   anticipate that this T-ALL-EC platform can contribute to elucidating leukemia-  
21   microenvironment interactions and identify effective compounds and therapeutic  
22   vulnerabilities.

1    **Introduction**  
2    T-cell acute lymphoblastic leukemia/lymphoma (T-ALL/LBL)<sup>1</sup> is an aggressive  
3    hematological malignancy with high treatment failure and poor overall survival  
4    (OS)<sup>2-4</sup>. Developments in therapy and stem cell transplants have improved event-  
5    free survival (EFS) rates of young patients (~80%). However, refractory/relapsed  
6    pediatric (~20%) and adult T-ALL (~40%) patients often die from disease<sup>5,6</sup>.

7              The original stratification of T-ALL (European Group for the Immunological  
8    Classification of Leukemia Scoring System - EGIL) highlights a class of early T-  
9    cell precursor acute lymphoblastic leukemia: ETP-ALL, representing ~5-15% of T-  
10   ALL. ETP patients have significantly worse survival<sup>7,8</sup>; a course recently improved  
11   via intensive asparaginase-based regimens<sup>5</sup>. Within T-ALL, the deregulated  
12   expression of multiple transcription factors, CDKN2A/2B cell-cycle regulators and  
13   hyperactive NOTCH1 signaling were initially described as key genomic  
14   aberrations. Furthermore, defects affecting JAK/STAT signaling, protein  
15   translation, and epigenetic control provide novel and attractive targets for  
16   therapy<sup>9-13</sup>. Of note, the implementation of transcriptional signatures is providing  
17   actionable diagnostic criteria and improved clinical management<sup>14</sup>.

18             The cancer microenvironment plays a critical role<sup>15-17</sup> in modulating cell  
19   growth and therapeutic responses<sup>16-19</sup>. Within the T-ALL niche, collective pro-  
20   tumorigenic signals arise from multiple cellular and non-cellular components.  
21   Notably, tumor-associated endothelial cells (TECs) are crucial in the pathogenesis  
22   of solid and liquid malignancies<sup>20-22</sup>, ultimately contributing to multiple pro-  
23   tumorigenic phenotypes. In T-ALL, TECs modulate leukemic extravasation<sup>23</sup> and  
24   tumor aggressiveness via multiple and synergistic mechanisms, including  
25   SDF1 $\alpha$ /CXCR4, DLL4-JAG1-2/NOTCH and IGFBP7/IGF1 pro-survival  
26   pathways<sup>18,24,25</sup>. However, it is unclear how these individual compartments  
27   contribute to the education of leukemic and microenvironment cells. Importantly,  
28   the microenvironment can affect drug responses<sup>15,26</sup> via dysregulated chemokine  
29   signals<sup>27</sup>, enhanced production of oxidative radicals and exosomes<sup>28</sup>, and  
30   hypoxia<sup>29</sup>. As a result, therapies targeting microenvironment cells are predicted to  
31   improve clinical responses<sup>30,31</sup>. However, the influence of endothelial-based  
32   cultures on perturbing drug responses has not been fully explored yet.

1       Taking advantage of endothelial cells (ECs) transduced with the E4ORF1  
2 (E4-ECs)<sup>32,33</sup>, we developed an endothelial-leukemia platform to explore the  
3 subverted role of tumor vascular niches. This platform integrates T-ALL patient-  
4 derived tumor xenografts (PDX) and ECs with drug screening libraries, ultimately  
5 translating findings to in-vivo preclinical trials. This approach led to the generation  
6 of proof of concept (PoC) transcriptional signatures that are predictive of drug  
7 response, and the selection of effective compounds/combinations in T-ALL. More  
8 importantly, we show that T-ALL and ECs bidirectionally modulate their  
9 transcriptomes and phenotypes, and ECs provide signals counteracting the  
10 efficacy of selected drugs.

11 Ultimately, we established an EC-based platform to unveil new microenvironment-  
12 leukemia interactions and cancer vulnerabilities. We anticipate that this approach  
13 could foster the design of precision medicine based approaches to improve the  
14 treatment of T-ALL patients.

15

## 16 **Methods**

### 17 **Patient material**

18 Pathological samples from bone marrow or peripheral blood (blasts >80%) were  
19 collected at the Hematology Center of “Sapienza” University of Rome or Weill  
20 Cornell Medicine of New York. Diagnoses were assigned according to the WHO  
21 classification. According to the Declaration of Helsinki, de-identified patients'  
22 samples were obtained with informed consent. The Institutional Review Boards of  
23 Sapienza University of Rome and Weill Cornell Medicine approved human  
24 studies.

25

### 26 **PDX generation**

27 PDX implantation and propagation were previously reported<sup>34</sup>. Briefly, fresh, or  
28 cryopreserved patients' samples were implanted into NOD.Cg-B2mtm1Unc  
29 Prkdcscid Il2rgtm1Wjl/SzJ (NSG B2m) mice. Animals were sacrificed when  
30 lymphoblastic cells represented ≥50% of the total circulating blood cells. Serial  
31 passages were achieved by i.v. injection into NOD Cg-Prkdc<sup>scid</sup> Il2rg<sup>tm1Wjl</sup>/SzJ

1 (NSG). Animal studies were approved by Weill Cornell Medicine Animal Care and  
2 Use Committee (2014-0024).

3 **Flow cytometry**

4 Flow cytometry was performed as described previously<sup>35</sup> using dedicated  
5 instrumentations (BD™ LSR II flow cytometer and BD FACSCelesta™ with plate  
6 reader for high-throughput screenings- HTS) and high-speed sorting (BD™ Aria).

7

8 **Cell culture, stimulating factors and drug screening**

9 PDX-derived T-ALL cells were cultured in RPMI with 10% FCS or StemSpan (SS;  
10 StemCell Technologies) supplemented with 10% knock-out Serum Replacement  
11 (KSR; Life Technologies), and a cocktail of antibiotics and interleukins (see  
12 Supplemental Data). Human umbilical vein endothelial cells transduced with E4-  
13 ORF1 gene (VeraVec EC; Angiocrine Bioscience), namely E4-ECs, were cultured  
14 in ex vivo media supplemented with 10% FCS (Lonza) and maintained at 37°C in  
15 a humidified 5% CO<sub>2</sub> atmosphere. Compounds for the drug screenings were  
16 purchased from Selleckchem (tested for 72hrs, at least in duplicates) at a  
17 concentration of 1.0µM or in dose-response dilutions where specified. The 433-  
18 drugs screenings were executed in 384-well plates using either RPMI (plus 10%  
19 FCS) or SS (plus 10% KSR) conditions, and the viability was assessed using the  
20 CellTiter GLO assay (Promega). The EC/T-ALL co-culture screenings were  
21 performed in 96-well plates, data were collected using the HTS flow cytometer.  
22 The gating strategy was based on appropriately compensated settings of the  
23 multicolor flow cytometry (PI for cell death, CFSE for EC labeling, and cell tracer  
24 violet for T-ALL cells). To provide uniform measures of drug effects and estimate  
25 EC-rescue, we computed specific cell death by normalizing viability upon drugs  
26 exposure with the viability of matched DMSO controls [formula: (death under drug  
27 x)-(death of control)/(100-death of control) \* 100]. Drugs were defined as active  
28 when able to kill >50% of leukemic cells compared to controls.

29

30 **Total RNA and single-cell RNA sequencing**

31 Refer to Supplemental Methods for details.

32

1

2

3 ***In-vivo treatment***

4 Mice were injected intravenously ( $1 \times 10^6$  T-ALL cells) and engraftment assessed  
5 by flow cytometric analysis of peripheral blood cells. When human T-cells reached  
6 5% of the total, mice were randomized into untreated (vehicle) and treated arms.  
7 Numbers, age, and gender of mice were equally distributed among arms.  
8 Compounds were administered as described in the Figure legends and in  
9 Supplemental Methods. Tumor burden was monitored by flow cytometric analysis  
10 of peripheral blood or spleen size using total body MRI or measurements post  
11 autopsy. Bodyweight was used as a surrogate for drug toxicity.

12

13 **Statistics**

14 The appropriate statistical methods were applied as indicated in the related Figure  
15 legends. Continuous variables were analyzed based on normal distribution and  
16 homogeneity of variance. Kaplan-Meier method and log-rank test were used to  
17 assess survival.

18 Tests were performed using GraphPad Prism (version 9.0; San Diego, California  
19 USA), MatLab (version 9.0, Natick MA) or R (version 4.0, The R Foundation for  
20 Statistical Computing 2020).

21

22 **Data sharing**

23 For original data, please contact ggi9001@med.cornell.edu.

24

25 **Results**

26 **Drug screening of T-ALL PDX identifies targetable vulnerabilities**

27 We first characterized the transcriptomic profile of 39 T-ALL patients' samples  
28 (Figure 1A), from which we established a library of PDX models (n=22) (Table S1,  
29 Figure S1A-C). These closely recapitulated the transcriptomic profile and shared  
30 identical the T-cell receptor (TCR) with those of matched patients (Figure 1B-C,  
31 Figure S1D, and Table S1).

32 We then implemented a multi-step approach including: 1) optimizing T-ALL  
33 PDX cells culture conditions ex-vivo; 2) screening a broad library of drugs; 3)

1 testing drug candidates in an EC-based co-culture system; and 4) confirming key  
2 candidates *in vivo* using PDX models.

3 Firstly, we tested various culture conditions and media, demonstrating  
4 improved viability and increased cell number in supplemented StemSpan (SS)  
5 medium relative to supplemented RPMI media (Figure S1E).

6 Secondly, we challenged T-ALL PDX cells *ex-vivo* with a drug library of 433  
7 compounds (1uM), targeting ~634 proteins (Figure 1D-F and Table S2). Prior to  
8 choosing the 1uM final concentration, we verified that IC50 would be reached in  
9 most of the compounds (400/433, 92%). In detail, 13 samples spanning different  
10 passages of six T-ALL PDX models were tested. We observed high reproducibility  
11 among biological and technical replicates (Figure S1F-I). StemSpan (SS)-cultured  
12 PDX cells showed that most compounds (~89%) had little-to-no effect on T-ALL  
13 viability. Meanwhile, only 11% of drugs reduced the average cell viabilities across  
14 PDX models to less than 50%, corresponding to a cluster of 39 drugs (Figure 1F).  
15 To further elaborate on the drug concentration (1uM), we tested serial dilutions of  
16 10/39 broadly active compounds in four additional PDX models, identifying unique  
17 IC50 in individual models (Figure S1P). In all cases, 1uM was compatible with the  
18 efficacy range.

19 Using unsupervised hierarchical clustering and Principal Component  
20 Analysis (PCA), we demonstrated two clusters of T-ALL samples based on  
21 differential drug susceptibility (Figure 1G). Specimens belonging to earlier  
22 passages populated cluster 1 (C1), whereas later passages were more often  
23 skewed towards cluster 2 (C2), suggesting a decreased therapeutic efficacy along  
24 serial passages (Figure S1I). We confirmed this passage-induced reduced  
25 viability using 3053 T-ALL PDX (Figure S1J), in which we identified the  
26 enrichment of the SMCHD1-JAK2 fusion overtime (Figure S1K-M). To describe  
27 the response heterogeneity among the different T-ALL models, we combined the  
28 viability results of 3119/3053 and R05/RO6 T-ALL PDX based on the highest  
29 response similarity scores (Figure S1N) identifying differentially active drugs  
30 between the two groups (Figure 1H, Figure S1O). Lastly, we attempted to  
31 correlate gene expression with drug responses, seeking to highlight drug-related  
32 biomarkers. Despite the limited number of samples, we identified several gene

1 signatures predictive of drug responses (Figure 1I and S1Q-R).

2

3 **Endothelial cells provide pro-survival signals and modulate the drug**  
4 **responses of T-ALL cells**

5 Within the tumor microenvironment, endothelial cells (ECs) sustain hematopoietic  
6 and neoplastic cells<sup>36,37</sup> and enhance their survival under toxic stress<sup>17,18,25,38,39</sup>.  
7 We previously demonstrated that primary non-transformed E4ORF1-transduced  
8 ECs<sup>32</sup> (herein referred to as E4-ECs) are an instructive serum-free/xenobiotic-free  
9 model to study tumor-host interactions<sup>25</sup>. Here, we first showed that E4-ECs  
10 sustained T-ALL cells in stress conditions such as starvation, lymphokine  
11 depletion, and oxygen deprivation (Figure S2A-E). We then developed a high-  
12 throughput flow-cytometry-based endothelial-leukemia co-culture system. Violet-  
13 tracer-labeled T-ALL cells from 10 PDX models were cultured in SS media  
14 supplemented with 10% KSR and challenged with the most effective drugs (n=39)  
15 from the initial screening (n=433) in the presence of CFSE-labeled E4-ECs  
16 (Figure S2F).

17 Sensitivity data showed a high concordance among T-ALL cells isolated  
18 from separate compartments (spleen and bone marrow) from the same PDX  
19 mouse (Figure S2G), from sibling mice implanted with the same tumor seeds  
20 (Figure S2H), and from mice belonging to two consecutive passages (Figure S2I).  
21 Additionally, the percentage of viable E4-EC cells cultured alone and/or with T-  
22 ALL cells was similar across all compounds (Table S5). These findings suggested  
23 that T-ALL responses likely were not linked to suboptimal drug concentrations  
24 (Figure S2J).

25 Overall, E4-ECs significantly improved the T-ALL survival of individual PDX  
26 models against selected compounds after 72hr ex-vivo treatment (Figure 2A-D  
27 and Figure S2K). A compound was defined as “rescued” when there was a  
28 decrease of  $\geq 20\%$  in specific cell death compared to no-EC condition. By PCA,  
29 the vectorized EC-rescue showed converging direction in all models, suggesting  
30 conserved rescue mechanisms (Figure 2A-B and Figure S2K). Of note, some  
31 compounds were reproducibly rescued across multiple PDX models, (including  
32 oligomycin, JQ1, NSC319726, SN38, belinostat, CEP-18870, KPT-185, SC144,

1 TSA and YM155). Others were poorly effective in specific models, underlying  
2 potential “private” rescue mechanisms (Figure 2C-D and Figure S2L-M). Further,  
3 we tested 12 additional drugs on 7/10 PDX models screened, including  
4 conventional chemotherapeutics for T-ALL and novel compounds in clinical trials  
5 (Figure S2N). We identified commonly rescued drugs (asparaginase,  
6 dexamethasone, vincristine, ponatinib, dasatinib, and YKL-5-124 [CDK7 inhibitor],  
7 4 models). Overall, rescued compounds were active on molecules belonging to  
8 interconnected pathways, such as PI3K-Akt, p53, FoxO, JAK-STAT, NOD-like  
9 receptor, HIF-1 (Figure S2M). Next, we computed a modified Shannon entropy for  
10 each PDX model (see Methods) (Figure 2E), showing an overall tendency  
11 towards increased response heterogeneity and plasticity in the presence of E4-  
12 ECs. We then focused on the different response profiles of the 10 PDX models  
13 challenged in the presence of E4-ECs. Among the most effective drugs across all  
14 models, some are of particular interest due to their potential clinical applicability:  
15 proteasome inhibitors (bortezomib, CEP18870, MLN2238; average SCD: 83%,  
16 79% and 78% respectively) HDAC inhibitors (panobinostat, belinostat, CHIR124;  
17 average SCD: 75%, 69% and 51% respectively), HSP-90 inhibitor (ganetespib,  
18 average SCD: 49%), BCL2 inhibitors (venetoclax and navitoclax, average SCD:  
19 27% and 66% respectively). Notably, other drugs displayed unique efficacy in  
20 selected models and against different T-ALL phenotypes, with ETP-ALL samples  
21 showing increased resistance to several compounds (Figure 2F, Figure S2O-R):  
22 YM155 (survivin inhibitor; delta SCD ETP-non ETP= 39.9%, p<0.0001), SNS032  
23 (CDK2/9 inhibitor, delta SCD= 34.7%, p=0.01), Ouabain (ATP1A1 inhibitor, delta  
24 SCD= 31%, p=0.02), STF118804 (NAMPT inhibitor, delta SCD= 20.9%) and KPT-  
25 185 (XPO1 inhibitor, delta SCD= 17.2%, p<0.0001).

26 Finally, we used our dual T-ALL-EC platform to test targets based on the  
27 genetic background of individual T-ALL PDX. We treated 3119 PDX cells (carrying  
28 a NUP14/ABL translocation) with dasatinib, and RO2 PDX cells (mutant JAK1-  
29 JAK3-STAT5B) and RO6 PDX cells (mutant STAT5) (Table S1) with Jak inhibitors  
30 (ruxolitinib and tofacitinib, alone or in combination), in the presence or absence of  
31 E4-ECs (Figure S2S). E4-ECs partially rescued T-ALL cells from single-agent  
32 treatments. However, in combination, ruxolitinib and tofacitinib were significantly

1 more effective in both RO2 and RO6 PDX.

2 These results highlighted the utility of the T-ALL-EC platform to assess: 1)  
3 drugs that are effectively rescued by EC; 2) pathways collectively or privately  
4 involved in EC-rescue; 3) differential T-ALL response profiles based on intrinsic  
5 tumor features, and 4) unique targetable T-ALL vulnerabilities.

6

7 **T-ALL and EC reciprocally modulate their transcriptomics signatures**

8 Aiming to elucidate the relationships between EC and T-ALL cells, we  
9 investigated the transcriptomic profiles of co-cultured E4-ECs and T-ALL cells  
10 from 3119 and RO2 PDX models using single-cell RNA sequencing (scRNA-seq).  
11 After QC filtering (Figure S3A), we clustered all cells based on differentially  
12 expressed genes and compartment identity (Figure 3A, Figure S3B-D). We  
13 analyzed 3119 and RO2 T-ALL PDX models separately, given their divergent  
14 genetic profiles (Table S1). Notably, proliferating T-ALL cells were most frequently  
15 included in clusters enriched in EC-co-cultured T-ALL cells in both models (Figure  
16 3B and Figure S3E). We found that T-ALL co-cultured with E4-ECs underwent  
17 profound transcriptional changes (Figure 3C, Table S6). Furthermore, the  
18 differentially expressed genes defined an EC-mediated “T-ALL education  
19 signature” for each model, with significant overlap between the two models and a  
20 high concordance with bulk-RNAseq data from cells cultured in the same  
21 conditions (Figure 3D, S3F-G). In addition, we detected enhanced single-cell  
22 entropy in T-ALL co-cultured with E4-ECs (Figure S3H), accounting for increased  
23 plasticity<sup>40,41</sup>.

24 Then, we compared differential pathways activation between the two  
25 conditions. Both EC-cocultured RO2 and 3119 T-ALL cells upregulated JAK-  
26 STAT, MAPK, TGFB, and EGFR pathways, with downregulations of p53 signaling  
27 (Figure 3E). In addition, GSEA showed enrichment of the c-Myc pathway in co-  
28 cultured elements (Figure S3I), along with an increased expression of genes  
29 belonging to the NOTCH pathway (NOTCH3, HES1, HES4)<sup>42,43</sup> (Figure 3F).  
30 Notably, IGF1R was also commonly upregulated in co-cultured T-ALL cells in both  
31 models (Figure 3F and S3J). Other commonly upregulated genes included:  
32 ribosomal genes RPS6 (highly expressed in several solid cancers<sup>44</sup> and in

1 immature leukemic blasts)<sup>45</sup>, RPL11 (whose activating mutations have been  
2 described in T-ALL)<sup>46</sup> and HMGB2, a known poor prognostic factor in several  
3 cancers<sup>47,48</sup>. In both models, MALAT1 (known to control the crosstalk between  
4 ECs and tumor cells<sup>49</sup>) was identified as one of the most downregulated gene in  
5 E4-EC-cocultured T-ALL. Similarly RHOH<sup>50</sup> (Figure 3C and F), normally  
6 expressed in hematopoietic cells where it functions as a negative regulator of cell  
7 growth and survival was also downregulated. Importantly, these differences were  
8 maintained at single-cell resolution, allowing us to define model-specific clusters  
9 with enrichment of educated cells (RO2: cluster 5; 3119: clusters 0 and 4) (Figure  
10 3F). Finally, to investigate whether E4-ECs could contribute to preserving a more  
11 immature/stem-like phenotype, we evaluated the differential expression of genes  
12 linked to T-cell commitment and maturation<sup>51,52</sup>. In both models, EC-co-cultured T-  
13 ALL cells expressed higher levels of genes related to early double-negative (DN)  
14 or double-positive proliferating (DP-P) thymocytes. In contrast, T-ALL cultured  
15 alone were more shifted towards DP-quiescent (Q) or mature T-cell phenotypes  
16 (Figure 3G).

17

#### 18 **ECs in contact with T-ALL acquire maladapted TEC-like features**

19 We then focused on the transcriptomes of E4-ECs cultured alone or with T-ALL  
20 cells of 3119 and RO2 PDX models. Overall, we distinguished different clusters  
21 corresponding to T-ALL-co-cultured ECs (educated E4-ECs) or E4-ECs cultured  
22 alone (Figure 4A, S4A). These populations were transcriptionally distinct, leading  
23 to the construction of T-ALL mediated “EC education signatures” (Figure 4A,  
24 Table S7). Globally, co-cultured E4-ECs upregulated interferon-gamma and -  
25 alpha response hallmark pathways (Figure S4B), and increased the activity of  
26 multiple pathways, including JAK-STAT, NF-κB, TNFa, and VEGF-A (Figure 4B),  
27 with a concurrent increase in entropy reflecting in higher differentiation potency  
28 and plasticity (Figure S4C)<sup>40,41</sup>. At the gene level, co-cultured E4-ECs displayed  
29 enrichment in Notch signaling, angiogenesis (DLL1<sup>53</sup>, JAG1<sup>54</sup>, CD34), cell  
30 migration, and survival (ETS1, ETS2, and IGFBP4) genes (Figure 4C).  
31 Conversely, IGFBP7, a known IGF1R decoy with tumor suppression features in  
32 different cancer types<sup>55</sup>, CD63/TIMP-1 (involved in endothelial migration), CD9,

1 and S100A10 (regulating cell-cell interaction) were down-regulated in co-cultured  
2 E4-ECs (Figure 4C).

3 Then, we performed a ligand-receptor analysis in 3119 and RO2 PDX  
4 models to investigate the bidirectional crosstalk between T-ALL and E4-ECs  
5 (Figure 4D). This approach led to the identification of heterogeneous interactions,  
6 mainly co-shared by the two models (Figures 4D and S4D). Among them, the  
7 IGF1-IGF1R axis was significantly enriched (in brackets in Figure 4D). Since co-  
8 cultured T-ALL upregulated IGF1R, and conversely E4-ECs downregulated  
9 IGFBP7 (see above), we attempted to functionally verify whether the selective  
10 abrogation of the IGF1 pathway could impact the EC-mediated drug rescue. We  
11 tested the 39 pan-effective drugs (Figure 2C) w/wo the recombinant IGFBP7 (500  
12 ng/mL) in 3119 and 3053 PDX. Of note, IGFBP7 abrogated the E4-EC-mediated  
13 rescue of enzastaurin (PKC-beta inhibitor) and SC144 (GP130 inhibitor) in T-ALL  
14 PDX 3119 and 3053 models, and CHIR124 (Chk1 inhibitor) and YM155 (Survivin  
15 inhibitor) in T-ALL PDX 3119 (Figure S4E). As these drugs regulate the activity of  
16 IGF1R or its downstream effectors<sup>56-58</sup> (Figure S4F), we postulate that the EC-  
17 mediated rescue is in part mediated by the engagement of IGF1R of T-ALL cells.

18 To further explore the changes in T-ALL-co-cultured E4-ECs, we correlated  
19 their transcriptomics profiles with tumor ECs (TEC – directly sorted from tumor  
20 masses) and naïve normal/E4-ECs (Table S8). These analyses demonstrated that  
21 in-vitro educated E4-ECs and TECs share a set of differentially expressed genes,  
22 relative to normal E4-ECs (Figure 4E-F, S4G-H). These genes have been  
23 implicated in orchestrating invasion and metastasis (i.e., GSK3B, BRAF, STAT3,  
24 MET), genome instability (i.e., PTEN, BRAF, KEF1, ATM), angiogenesis (i.e.,  
25 FOXO3, CREBBP, HIF1A), and enabling immortality (i.e., CDK6, SPEN, TNKS).

26 Lastly, we looked for genes co-shared by both RO2 and 3119 PDX models  
27 whose expression contributed to the education signatures in both compartments  
28 (EC and T-ALL) (Figure 4G, S4I) (Table S9). Expectedly, genes linked to the EC  
29 and T-ALL compartments were distinct and displayed different functional modules  
30 (Figure 4G). Therefore, T-ALL-EC model is an informative and useful tool to probe  
31 EC-tumor interactions.

32

1    ***In-vitro* EC-educated T-ALL mirror *in-vivo* T-ALL cells**

2    To validate the data generated using the *in-vitro* co-culture platform, we  
3    performed scRNASeq on T-ALL cells from the 3119 PDX spleen (ex-vivo splenic  
4    T-ALL cells). We identified 4 clusters representative of the intratumor  
5    heterogeneity based on the differential expression of genes related to: cell cycle,  
6    MYC, PI3K/AKT signaling, and epithelial-mesenchymal transition (Figure S5A-C).  
7    Then, we enriched our analysis by including cells from the same source cultured  
8    for 5 days ex-vivo in SS media either with E4-ECs (*in-vitro* EC-educated T-ALL) or  
9    without E4-ECs (T-ALL alone) (Figure 5A). Overall, seven T-ALL cell clusters  
10   were identified (Figure 5B-C). Clusters 0 and 4 were enriched with T-ALL  
11   elements cultured without EC, clusters 1, 5 and 6 with T-ALL cultured with EC,  
12   and 2 and 3 with T-ALL cultured from spleen. Of note, clusters 2, 3, 5, and 6  
13   showed a great abundance of E4-EC-educated T-ALL or spleen T-ALL cells  
14   (Figure 5D); pointing to the closer similarity of these two compartments compared  
15   to T-ALL cultured alone. Notably, clusters 2 and 3 were highly enriched of  
16   proliferating cells (Figure S5D). Then, we applied the T-ALL education signature  
17   defined in the previous *in-vitro* experiment within each cluster (Figure 5E).  
18   Remarkably, *in-vivo* splenic T-ALL were globally more similar to *in-vitro* EC-  
19   educated T-ALL than T-ALL alone. This was more evident in clusters 0 and 4,  
20   containing enough cells belonging to all different entities (Figure 5F-G and S5E).  
21   Ultimately, splenic T-ALL cells recapitulated the different expressions of genes  
22   contributing to the education signatures of both 3119 and RO2 PDX models  
23   (Figure 5F-G, S5E). These data demonstrated the reliability of EC/T-ALL co-  
24   culture platform in recapitulating *in-vivo* conditions.

25

26    **Positive hits selected *in-vitro* are effective in pre-clinical trials**

27    To validate our stepwise drug screening platform *in-vivo*, we selected five  
28   compounds shown to be effective on T-ALL cells in the presence of E4-ECs  
29   (Figure 2A-C, S2O-P), effective in preclinical settings and/or targeting underlying  
30   PDX T-ALL liabilities. Panobinostat (HDAC), ruxolitinib (JAK1/2 inhibitor),  
31   tofacitinib (JAK1/2/3, TYK2 inhibitor), bortezomib (20s proteasome inhibitor) and  
32   SN38 (irinotecan metabolite, topoisomerase I inhibitor) were tested in 11 PDX

models, accounting for an overall number of 111 mice (Figure 6A-B). Overall, treated mice had a better prognosis than mice receiving vehicles (Figure 6B). Firstly, R02 and R06 T-ALL PDX mice were challenged with ruxolitinib alone or in combination with bortezomib (R02) or tofacitinib (R06) (Figure S6A). Treatments were well-tolerated, with no signs of toxicity (data not shown). Comparing treated and control mice, spleen size and percentage of leukemic circulating cells were significantly reduced (Figure 6C-D, S6B-C). Among the three single agents tested, ruxolitinib was least effective in reducing circulating disease in both models, while both combinations allowed for better disease eradication, more pronounced reduction in spleen volumes and improved overall survival (Figure 6C-E, S6B-E). Based on the ex-vivo co-culture drug screening, we identified SN38 (the active metabolite of irinotecan), as active in all models tested, despite an insufficient partial rescue by E4-ECs (death rate of T-ALL cells >50% compared to controls in all cases [mean SCD: 68%, range 54%-83%]; Figure 1F, 2C). Accordingly, we randomized 3053 and 3119 T-ALL PDX mice to receive either vehicle or irinotecan (20 mg/kg/day for 2 weeks) (Figure S6F). Total body MRI documented a normalized spleen size by day 15 in treated mice (Figure 6F). We also detected a reduced blood leukemia burden in treated mice up to 40 days and an improved overall survival (Figure 6G-H) (median OS: 103 days vs. 52, p=0.0002). No signs of overt toxicity were documented (Figure S6G).

Epigenetic targeting using the HDAC inhibitor panobinostat has been suggested as a potential therapy against T-ALL<sup>59</sup>, and this strategy was supported by our in vitro drug screening (Figure 1F, 2C). Thus, we executed a single-drug pre-clinical trial with panobinostat, in eight different T-ALL PDX models (Figure 6I, S6H). This treatment significantly improved OS (median OS: 117 vs 68, p=0.03) (Figure 6I) and decreased circulating T-ALL blasts (Figure 6J). Lastly, based on the finding that the IGF1-IGF1R axis is upregulated in EC-co-cultured T-ALL cells (Figure 3F, 4D and S3J) and that its inhibition downregulated EC-mediated rescue (Figure S4E), we evaluated a selective IGF1R inhibitor (linsitinib) in-vivo in four different PDX models (Figure 6K-L, S6I). As a debulking agent, we utilized daunorubicin, an identified pan-active compound in our drug screening in vitro (Figure 1F, 2C). The combination of daunorubicin + linsitinib

1 controlled disease more effectively and improved OS (median: 84 days)  
2 compared to single agents (median: 68 days daunorubicin; 63 days: linsitinib) or  
3 controls (median: 42 days) ( $p<0.0001$ ) (Figure 6K-L), suggesting that the IGF1-  
4 IGF1R inhibition counteracted leukemia progression in combination with standard  
5 chemotherapy.

6 These data demonstrated the predictive utility of our screening platform, for drug  
7 discovery process to identify active compounds and T-ALL dependencies.  
8

## 9 **Discussion**

10 Our study presents a novel endothelial/cancer platform to define targetable  
11 vulnerabilities and identify effective drugs against T-ALL cells, potentially  
12 applicable to other cancers. Although the treatment of T-ALL patients has  
13 considerably improved, relapsed T-ALL often remains incurable<sup>5,6</sup>. Recent pre-  
14 clinical studies provide encouraging approaches<sup>60-62</sup>, however therapeutic  
15 response does not always depend on pathogenetic mutations<sup>10,63</sup>, and pre-clinical  
16 trials are costly and require specialized units. We envisioned a multistep approach  
17 that integrates readouts from large drug screenings on PDX cells *ex vivo*, followed  
18 by “ad hoc” *in-vivo* cross-validation (Figure 6A). We first identified a group of  
19 broadly active compounds across all models tested and observed that increased  
20 drug resistance might arise along serial propagations. This should be further  
21 exploited to improve our understanding of therapeutic failures. Of interest, we  
22 could find a correlation between responses and *a-priori* transcriptional profiles for  
23 selected agents, a strategy that can provide new avenues to discover biomarkers  
24 predictive of responses.

25 It is well known that the tumor microenvironment can modulate drug  
26 responses in acute leukemia, a scenario epitomized by the contribution of  
27 mesenchymal and endothelial cells<sup>15-19</sup>. Specifically, ECs have been seldom  
28 utilized in broad drug discovery programs<sup>64</sup>. Nevertheless, their role in the  
29 maintenance/regulation of HSC<sup>36,37</sup> is well established, fostering ALL survival via  
30 a multitude of signaling pathways (i.e. Notch<sup>65</sup>, SDF-1<sup>66</sup> and CXCL12<sup>67</sup>).  
31 Accordingly, we generated a co-culture system using E4ORF1-transduced ECs,  
32 which have been proven to sustain T-ALL cells *in-vitro* and can be propagated for

1     $\geq$ 5-10 passages *in-vitro*. This system demonstrated that the T-ALL drug  
2    susceptibility was down-modulated by ECs. Single-cell analysis revealed that a  
3    multitude of ligand-receptor interactions and downstream pathways are involved  
4    in this process (e.g. IGF1/IGF1R, NOTCH-DLL and JAK/STAT), suggesting that  
5    EC-mediated pro-survival effect may require a multi-targeted approach to be fully  
6    counteracted. Toward this end, adding recombinant IGFBP7 *in-vitro* abrogated  
7    EC-rescue for selected compounds, suggesting reliance upon the IGF1-IGF1R  
8    pathway in specific cases.

9       On the other hand, several compounds were effective in the presence of  
10   ECs across multiple models. These included drugs with clinical interest  
11   (proteasome, HDAC, HSP-90, and BCL2 inhibitors). These results may be  
12   partially linked to unique T-ALL subgroups, with ETP-ALL being overall more  
13   resistant, specifically upon exposure to drugs targeting PI3K-AKT and JAK-STAT  
14   pathways. A selection of five compounds was ultimately shown to be effective *in-*  
15   *vivo* either alone or in combination. This was exemplified by irinotecan, a drug  
16   currently approved for treating many solid tumors, suggesting its potential  
17   repositioning in the context of T-ALL, and panobinostat, an HDAC inhibitor whose  
18   effect in T-ALL has not been fully unraveled. Similarly, the efficacy of JAK/STAT  
19   inhibitors has been documented in models carrying activating mutations, and in  
20   ETP-ALL<sup>10,13,68</sup>. Moreover, the data generated *in-vitro* with recombinant IGFBP7  
21   and the improved survival of daunorubicin-treated T-ALL PDX in combination with  
22   IGF1R inhibitor linsinitib (although limited on 4 models) further support the role of  
23   the IGF1/IGF1R signaling in the leukemia-EC crosstalk.

24       Mechanistically, we show that ECs and T-ALL cells undergo bilateral  
25   transcriptional changes modulating critical signaling pathways at the single-cell  
26   resolution. On the T-ALL side, these genes were mostly linked to stemness, T-cell  
27   commitment and maturation, emphasizing the heterogeneity and plasticity of  
28   leukemic elements. Remarkably, T-ALL co-cultured with E4-ECs were more  
29   similar to *ex-vivo* splenic T-ALL freshly harvested from PDX mice compared to T-  
30   ALL cells cultured alone, proving the reliability of our co-culture system. On the  
31   EC side, a significant set of differentially expressed genes were expressed in  
32   common with *in-vivo* TECs. These bidirectional changes are reflected in an

1 increased transcriptomic and pharmacological entropy, further pointing toward the  
2 dynamicity of this dual-culture system compared to conventional static suspension  
3 cultures.

4 Hence, EC-T-ALL co-culture system partially recapitulates *in-vivo*  
5 conditions, representing a robust platform to study leukemia-host interactions and  
6 drug sensitivities. We envision that this integrated stepwise approach might  
7 overcome the liabilities of current drug screenings and propel the entry of new  
8 agents and combinations in clinical trials.

1   **Financial support**

2   This work was supported in part by the Italian Association for Cancer Research  
3   (AIRC, Milan, Italy), Metastases 5x1000 Special Program, grant 21198 to Robin  
4   Foa; CA229086, CA229100, LLS 7011-16, Departmental funds and the Sandra  
5   and Edward Meyer Cancer Fund to Giorgio Inghirami; and the Rita-Levi Montalcini  
6   grant from Italian Ministry of University and Research (MIUR) to Danilo Fiore.  
7   Jude M Phillip is supported by NIH grant R01CA187109-03S1 and Luca Vincenzo  
8   Cappelli by American Italian Cancer Foundation (AICF) Post-Doctoral Research  
9   Fellowship.

10

11   **Acknowledgements**

12   We thank Dr. J. Casano, and A. Miyaguchi for their technical support and A.  
13   Arkur, and S.B. Shah for their administrative assistance. We are grateful to the  
14   Weill Cornell Medical College Epigenomics for generation sequencing (NGS)  
15   library preparation and sequencing for this study. We also thank the members of  
16   the Weill Cornell Cell Sorting core and Edward Meyer Cancer Center PDX Shared  
17   Resource.

1   **Authorship Contributions**  
2   **L. V. Cappelli:** Conceptualization, formal analysis, methodology, writing-original  
3 draft, writing-review and editing. **D. Fiore:** Conceptualization, formal analysis,  
4 methodology, writing-original draft, writing-review and editing. **J.M. Phillip:**  
5 Conceptualization, formal analysis, methodology, writing-original draft, writing-  
6 review and editing. **L. Yoffe:** Conceptualization, formal analysis, methodology,  
7 writing-original draft, writing-review and editing. **F. Di Giacomo:**  
8 Conceptualization, formal analysis, methodology, writing-original draft, writing-  
9 review and editing. **Y. Hu:** Formal analysis, methodology, editing. **C. Kayembe:**  
10 Formal analysis, methodology, editing. **W. Chiu:** Formal analysis,  
11 methodology. **M. Ginsberg:** Conceptualization, formal analysis, methodology,  
12 editing. **L. Consolino:** Conceptualization, formal analysis, methodology,  
13 editing. **J.G.B Duran:** Conceptualization, methodology, editing. **N. Zamponi:**  
14 Conceptualization, formal analysis, methodology, editing. **A.M. Melnick:**  
15 Conceptualization, writing-review and editing. **W. Tam:** Conceptualization, formal  
16 analysis, methodology, writing-original draft, writing-review and editing. **O.  
17 Elemento:** Conceptualization, formal analysis, writing-review and editing. **S.  
18 Chiaretti:** Conceptualization, writing-review and editing. **A. Guarini:**  
19 Conceptualization, writing-review and editing. **R. Foa:** Conceptualization, writing-  
20 review and editing. **L. Cerchietti:** Conceptualization, formal analysis,  
21 methodology, writing-original draft, writing-review and editing. **S. Rafii:**  
22 Conceptualization, formal analysis, methodology, writing-original draft, writing-  
23 review and editing. **G. Inghirami:** Conceptualization, data curation, formal  
24 analysis, supervision, methodology, writing-original draft, project administration,  
25 writing-review and editing.  
26

27   **Conflict of interest**

28 Michael Ginsberg is currently employed at Angiocrine Bioscience, San Diego, CA,  
29 USA.  
30 Shahin Rafii is a co-founder and non-paid consultant to Angiocrine Biosciences,  
31 San Diego, CA, USA.  
32 The other authors declare no potential conflicts of interest.  
33

1    **Figure Legends**

2

3    *Graphical abstract*

4    Representative scheme of in-vitro drug discovery coupled with an in-vivo  
5    preclinical trial. Tumor cells from PDX are first screened with a 433 library of  
6    compounds in 384-well format. Positive hits are then validated in 96-well plates  
7    with and without E4-ECs. Compounds with therapeutic efficacy against T-ALL but  
8    neutral to E4-ECs are lastly tested in-vivo against PDX cells.

9

10

11    **Figure 1. High-throughput screening of T-ALL patient-derived tumor**  
12    **xenografts (PDX) defines therapeutic responses *ex vivo*.**

13

14    (A) Principle component analysis of 39 T-ALL primary samples separated into two  
15    major subgroups corresponding to ETP and canonical T-ALL. A third group  
16    with intermediate phenotype could also be identified.

17    (B) Unsupervised hierarchical clustering of RNA expression profiles among 10 T-  
18    ALL PDXs sequenced over multiple passages, including primary (PR) and  
19    serial (T) samples.

20    (C) Principal component analysis of 10 T-ALL PDXs sequenced over multiple  
21    passages, including primary (PR) and serial passages.

22    (D) Scheme illustrating the drug screening of T-ALL PDXs exposed to 433 drugs  
23    with *in silico* processing and analysis.

24    (E) Dotplot showing drug responses as a function of media for two consecutive *in-*  
25    *vivo* passages (RPMI with 10% FCS vs. StemSpan [SS] with 10% KSR and  
26    interleukins) for a representative PDX (3053 T-ALL model).

27    (F) Heatmap showing the overall responses assessed using ATPGlo assay of 6  
28    different PDXs (14 samples corresponding to multiple passages) across 433  
29    drugs screened in SS for 72hrs in duplicate (red, hits—low viability; white,  
30    viabilities greater than or equal to vehicle control). Dendograms on the left  
31    and bottom show the unsupervised hierarchical clustering of drugs and PDX  
32    samples along the axis of maximum variation (ward) of the Euclidean  
33    distances. The bar plot on the top shows the pan-drug viabilities per sample  
34    across all 433 drugs, with error bars highlighting the standard deviation. Bar  
35    plot on the right shows the pan-sample viability per drug, with the gray trend  
36    line highlighting the magnitude of the coefficient of variance. Orange inset  
37    highlights a subset of the 39 most active drugs across all PDX models, listed  
38    on the right panel with average viabilities shown as a bar plot and error bars  
39    showing the standard deviation.

40    (G) PCA of 14 PDX samples based on the responses to all 433 drugs in the  
41    screening library (left panel). Dendrogram for the same samples showing  
42    unsupervised clustering based on the responses of the drug screening library  
43    (right panel). Two components (C1 and C2) were identified, corresponding to  
44    increased resistance of T-ALL cells with passaging over time in mice.

45    (H) Volcano plot showing differential viability versus the inverse deviation score,  
46    highlighting differentially active drugs in R05/R06 vs 3119/3053 T-ALL PDX  
47    models. Green dots on the left indicate drugs more active in R05/R06,

1 magenta dots on the right denote drugs that are more active in 3119/3053 T-  
2 ALL models, and gray dots indicate equally active drugs.

3 (I) Heatmap and unsupervised clustering depicting gene expression within the  
4 PI3K-AKT signaling pathway, targeted by HSP-90 inhibitor Ganetespib. Genes  
5 were selected based on a significant correlation between their expression  
6 across samples and the viability of the treated sample. The viability values are  
7 indicated in the color bar on the right.

1   **Figure 2. ECs provide pro-tumorigenic signals to T-ALL cells.**  
2   (A) Principal component analysis (PCA) plot showing the responses of 10  
3   individual T-ALL PDX models cultured with and without ECs connected by vectors  
4   depicting the trajectory of the EC-rescue.  
5   (B) Scatter plot showing the differential specific cell death between samples co-  
6   cultured with E4-ECs vs alone for the ten models from (A). P-value was estimated  
7   with T-test.  
8   (C) Heatmap showing the differential responses of 10 T-ALL PDX models in the  
9   presence or absence of ECs. Color coding corresponds to the specific cell death  
10   (SCD) delta of the +EC minus the -EC conditions (here referred to as Efficacy +/-  
11   EC). Red color indicates drugs that are rescued by EC while blu color those that  
12   produce more death in the presence of ECs.  
13   (D) Pie charts indicating the drugs having greater than 20% EC-mediated rescue  
14   for the 10 T-ALL PDX models.  
15   (E) Box and whisker plots showing the heterogeneity score (calculated as a  
16   modified Shannon entropy) per T-ALL PDX model in the presence or absence of  
17   ECs.  
18   (F) Boxplot showing specific cell death (SCD) upon exposure to the 39 most  
19   active compounds from the library in either ETP (yellow bars) or non-ETP (grey  
20   bars) models (median and standard error). The central area represents drugs that  
21   are equally effective between the two subgroups, the leftmost part those that are  
22   more efficient in ETP and the rightmost part in non-ETP T-ALL. The delta SCD is  
23   color coded at the bottom of the bars. Right insert: volcano plot of the same data  
24   depicting -log10 p value corrected for multiple comparison (y axis) and delta SCD  
25   of ETP minus non-ETP samples. The upper-left corner depicts drugs that are  
26   significantly less effective in ETP, the upper-right corner in non-ETP models.

1   **Figure 3. T-ALL cells are modulated by E4-ECs in vitro.**  
2   (A) UMAP plots and cell clustering of single-cell RNA-seq of T-ALL cells and E4-  
3   ECs. Freshly isolated T-ALL PDX cells were cultured alone or with E4-ECs.  
4   Single-cell RNA-seq was performed on day 5. Upper panels are color-coded by  
5   cluster identity, bottom panels depict barplots of sample identity in each cluster.  
6   (B) UMAP plots of single-cell RNA-seq of T-ALL cells color coded by cell cycle  
7   (G1, S and G2M phase) (upper panels). Barplots showing the different proportions  
8   of cells in G1/S/G2M phase based on cluster identity for both RO2 and 3119 T-  
9   ALL PDX models (bottom panels).  
10   (C) Heatmap showing the differentially expressed genes from single-cell RNA-seq  
11   of RO2 and 3119 T-ALL model cultured either alone or with E4-ECs. The top 50  
12   up- and down-regulated genes are depicted for each model.  
13   (D) UMAP and violin plots displaying T-ALL “education scores” calculated based  
14   on differentially expressed genes from (C). The scores are applied to each cluster  
15   to identify those with an enrichment in “educated” T-ALL cells.  
16   (E) Heatmap depicting the pathways activity levels determined using PROGENy  
17   tool applied on single-cell RNA seq data of RO2 and 3119 T-ALL cells cultured  
18   alone or in co-culture with E4-ECs.  
19   (F) Dot-plot displaying expression levels of a selected set of genes across  
20   different single-cell clusters composed of RO2 and 3119 T-ALL PDX cells cultured  
21   alone or with E4-ECs. The size of the dot indicates the percentage of cells  
22   expressing each gene, color-coded by expression level. Expression levels were  
23   measured using log-normalized counts. Green squares indicate clusters enriched  
24   of EC-co-cultured T-ALL elements, while red ones clusters mainly consisting of T-  
25   ALL cultured alone.  
26   (G) Dot-plot depicting expression levels of a signature of genes involved in T-cell  
27   maturation and commitment in T-ALL cells from RO2 or 3119 cultured with/without  
28   E4-ECs (from <sup>51,52</sup>). The size of the dot indicates the percentage of cells  
29   expressing each gene, color-coded by expression level. Expression levels were  
30   measured using log-normalized counts. Legends (from <sup>51</sup>) = DN early: double  
31   negative (CD4/CD8<sup>-/-</sup>) -early T-cell; DN (P): double negative proliferating T-cells;  
32   DN (Q): double negative quiescent T-cells; DP (P): double positive proliferating T-  
33   cells; DP (Q): double positive quiescent T-cells.

1 **Figure 4. E4-ECs in contact with T-ALL establish a maladapted niche and**  
2 **acquire TEC-like features.**

3 (A) Heatmap of the top 50 up- and down-regulated genes from single-cell RNA-  
4 seq in EC alone or after co-culture with T-ALL elements in both RO2 and 3119  
5 PDX models.

6 (B) Heatmap depicting the pathways activity levels determined using PROGENy  
7 tool applied on single-cell RNA seq data of E4-ECs cultured alone or in co-culture  
8 with 3119 and RO2 T-ALL cells.

9 (C) Dot-plot displaying expression levels for a set of genes of interest (DLL1,  
10 JAG1, CD34, ETS1, ETS2, IGFBP4, IGFBP7, CD63, CD9 and S100A10) in E4-  
11 ECs that were cultured alone or in co-culture with RO2 and 3119T-ALL elements.  
12 The dot size encodes the percentage of cells expressing each gene, and the color  
13 encodes the average expression level across all cells. Expression levels were  
14 measured using the log-normalized counts.

15 (D) Circos plot of ligand-receptor interaction obtained through CellPhoneDB  
16 package on RO2 PDXmodel, based on the relative expression level measured by  
17 single-cell RNA seq. Only the significant associations between ligands and  
18 receptors (on either the T-ALL or the EC sides) are depicted.

19 (E) List of a set of genes commonly up-regulated by tumor endothelial cells (TEC)  
20 (vs normal ECs) and by E4-ECs co-cultured with T-ALL cells (vs cultured alone)  
21 (see F). The list of processes and functions involving each gene was derived from  
22 NDEx Biological Network Repository.

23 (F) Venn diagram showing the comparison of genes up-regulated in TEC vs.  
24 normal E4-ECs (green circle) and in educated vs naïve E4-ECs (blue circle). P-  
25 value was calculated using a hypergeometric test.

26 (G) List of a set of genes up- or down-regulated by E4-EC and T-ALL co-cultured  
27 vs cultured alone in common between the two PDX models (RO2 and 3119)  
28 (Figure S4I). The direction of the differences is color-coded (blue: down-regulated;  
29 red: up-regulated). The list of processes and functions involving each gene was  
30 derived from NDEx Biological Network Repository.

1   **Figure 5. In-vitro EC-co-cultured T-ALL mirror *in-vivo* T-ALL cells.**  
2   (A) Schematic representation of the single-cell RNA-seq analysis of 3119 T-ALL  
3   cells. Cells that were either cultured alone or co-cultured with E4-ECs in-vitro for  
4   five days were sequenced and combined with T-ALL cells freshly harvested from  
5   the spleen of a 3119 PDX mouse.  
6   (B) UMAP plot of the single-cell RNA-seq data derived from (A) color-coded by  
7   cluster identity.  
8   (C) UMAP plot of the single-cell RNA-seq data derived from (A) color-coded by  
9   sample origin.  
10   (D) Barplot showing the proportions of in-vitro and in-vivo T-ALL cells (A) based  
11   on cluster identity.  
12   (E) Violin plots showing the enrichment score of the education signature derived  
13   from the in-vitro experiment of 3119 PDX model (Figure 3D). In vitro EC-co-  
14   cultured and splenic T-ALL cells displayed similar enrichment across all clusters.  
15   (F) Dot-plot displaying expression levels for a set of genes in common between  
16   RO2 and 3119 T-ALL “educated” elements (Figure 4G, T-ALL genes) in ex-vivo  
17   splenic T-ALL cells compared to in vitro T-ALL elements (E4-EC-co-cultured and  
18   cultured alone). The expression of these genes was very similar in splenic and  
19   E4-EC-co-cultured T-ALL cells compared to T-ALL cultured alone, demonstrating  
20   that in-vitro EC-educated elements are more similar to those freshly harvested ex-  
21   vivo. The dot size encodes the percentage of cells expressing each gene, and the  
22   color encodes the average expression level across all cells. Expression levels  
23   were measured using the log-normalized counts.  
24   (G) Heatmap of the genes from 3119 “education signature” (Figure 3D) applied to  
25   cluster 0 from (B) containing enough cells from all three compartments (*in-vitro* T-  
26   ALL cultured alone vs with E4-ECs and *ex-vivo* splenic T-ALL). Cell proportions in  
27   cluster 0 are found in (D). T-ALL cells from the spleen are clustered together with  
28   EC-co-cultured T-ALL cells based on the expression of the education signature.

1   **Figure 6. Efficacy of positive hits from stepwise drug discovery approach *in-vivo*.**

2   (A) Representative scheme of our stepwise drug discovery approach coupled with  
3   in-vivo preclinical trials. Tumor cells from T-ALL PDX were first screened with a  
4   library of 433 compounds in 384-well plate format. Positive hits were then  
5   validated in 96-well plate format with and without E4-ECs. The number of  
6   candidates was narrowed down (n=30) after implementation of multiple  
7   experimental conditions and validations. Representative drugs not rescued by E4-  
8   ECs were then tested in-vivo and proved to be effective in T-ALL PDX mice.  
9   Depiction of the top-rank compounds is provided in the circle, clustered by their  
10   target(s) in relation with all the others (kmeans clustering with n=4 and  
11   confidence=0.65). Network edges thickness indicates the strength of data  
12   support.

13   (B) Kaplan-Meier plot depicting overall survival of all the mice (n=111) treated with  
14   vehicle vs different therapeutic regimens across 11 different PDX models. P-value  
15   was calculated using a log-rank test.

16   (C) Barplot showing the fold change of the percentage of T-ALL cells in blood of  
17   RO2 and RO6 PDX mice treated with ruxolitinib, bortezomib, tofacitinib and  
18   combinations compared to controls. P-values were calculated with T-test.  
19   \* $p<0.05$ , \*\* $p<0.01$ .

20   (D) Barplot showing the fold change of the spleen volume (measured by MRI) of  
21   RO2 and RO6 mice treated with ruxolitinib, bortezomib, tofacitinib and  
22   combinations compared to controls. P-values were calculated with T-test.  
23   \* $p<0.05$ , \*\* $p<0.01$ .

24   (E) Kaplan-Meier plot depicting overall survival of RO6 mice treated with vehicle,  
25   toccitinib, ruxolitinib or combination. P-value was calculated using a log-rank test.

26   (F) Line-dotplot showing changes in spleen volume (measured by MRI) of 3053  
27   PDX mice treated with irinotecan (20 mg/kg/day) compared to controls in a  
28   timeframe of 40 days. P-value was calculated with T-test. \*\*\*\* $p<0.0001$ .

29   (G) Line-dotplot showing changes in percentage of T-ALL cells in blood of 3053  
30   and 3119 PDX mice treated with irinotecan compared to controls in a timeframe of  
31   80 days. Three out of 12 irinotecan-treated mice relapsed and experienced death  
32   for leukemia. P-value was calculated with T-test. \*\*\*\* $p<0.0001$ .

33   (H) Kaplan-Meier plot depicting overall survival of 3053 and 3119 PDX mice  
34   treated with vehicle or irinotecan. Nine out of 12 irinotecan-treated mice died  
35   without leukemia. P-value was calculated using a log-rank test.

36   (I) Kaplan-Meier plot depicting overall survival of eight different T-ALL PDX  
37   models (6467, 14741, 7072, 7155, 13002, 13356, 10512 and 5384) treated with  
38   vehicle or HDAC inhibitor panobinostat (n=2 mice per arm, n=32 mice total) (5  
39   mg/kg/day). Mice belonging to 3/8 models (5384, 7155 and 6467) died without  
40   leukemia. P-value was calculated using a log-rank test.

41   (J) Barplot depicting the circulating T-ALL cells (delta day 30-day 0; day 0: first T-  
42   ALL detection in the blood) in eight PDX models treated with vehicle or  
43   panobinostat. A single partially refractory model was identified (1/8, 7072 PDX T-  
44   ALL). P-value was calculated with T-test. \*\* $p<0.001$ .

45   (K) Barplots depicting the percentage of circulating T-ALL cells in four PDX  
46   models (10512, 6467, 13002 and 13356) treated with vehicle, daunorubicin (1.2  
47   mg/kg for three days/week), linsitinib (50 mg/kg/day) or combination (n=2 mice  
48

1 per arm, n=32 mice total). Mice treated with daunorubicin + linsitinib displayed  
2 delayed leukemia progression compared to the other arms. P-value was  
3 calculated with T-test. \*p<0.05.  
4 (L) Kaplan-Meier plot depicting overall survival of 10512, 6467, 13002 and 13356  
5 T-ALL PDX models treated with vehicle, daunorubicin, linsitinib or combination.  
6 Mice treated with daunorubicin + linsitinib survived until 3 months from enrollment.  
7 P-value was calculated using a log-rank test.

1      **References**

- 2
- 3    1. Swerdlow SH, International Agency for Research on Cancer., Organization.  
4    WH. WHO classification of tumours of haematopoietic and lymphoid tissues (ed  
5    Revised 4th). Lyon, France: International Agency for Research on Cancer; 2017.
- 6    2. Bassan R, Hoelzer D. Modern therapy of acute lymphoblastic leukemia. *J Clin Oncol.* 2011;29(5):532-543.
- 7
- 8    3. Guru Murthy GS, Pondaiah SK, Abedin S, Atallah E. Incidence and survival  
9    of T-cell acute lymphoblastic leukemia in the United States. *Leuk Lymphoma.*  
10   2019;60(5):1171-1178.
- 11   4. Pui CH, Robison LL, Look AT. Acute lymphoblastic leukaemia. *Lancet.*  
12   2008;371(9617):1030-1043.
- 13   5. Conter V, Valsecchi MG, Buldini B, et al. Early T-cell precursor acute  
14   lymphoblastic leukaemia in children treated in AIEOP centres with AIEOP-BFM  
15   protocols: a retrospective analysis. *Lancet Haematol.* 2016;3(2):e80-86.
- 16   6. Pui CH, Pei D, Cheng C, et al. Treatment response and outcome of  
17   children with T-cell acute lymphoblastic leukemia expressing the gamma-delta T-  
18   cell receptor. *Oncoimmunology.* 2019;8(8):1599637.
- 19   7. Jain N, Lamb AV, O'Brien S, et al. Early T-cell precursor acute  
20   lymphoblastic leukemia/lymphoma (ETP-ALL/LBL) in adolescents and adults: a  
21   high-risk subtype. *Blood.* 2016;127(15):1863-1869.
- 22   8. Morita K, Jain N, Kantarjian H, et al. Outcome of T-cell acute lymphoblastic  
23   leukemia/lymphoma: Focus on near-ETP phenotype and differential impact of  
24   nelarabine. *Am J Hematol.* 2021;96(5):589-598.
- 25   9. Cullion K, Draheim KM, Hermance N, et al. Targeting the Notch1 and  
26   mTOR pathways in a mouse T-ALL model. *Blood.* 2009;113(24):6172-6181.
- 27   10. Maude SL, Dolai S, Delgado-Martin C, et al. Efficacy of JAK/STAT pathway  
28   inhibition in murine xenograft models of early T-cell precursor (ETP) acute  
29   lymphoblastic leukemia. *Blood.* 2015;125(11):1759-1767.
- 30   11. Chonghaile TN, Roderick JE, Glenfield C, et al. Maturation stage of T-cell  
31   acute lymphoblastic leukemia determines BCL-2 versus BCL-XL dependence and  
32   sensitivity to ABT-199. *Cancer Discov.* 2014;4(9):1074-1087.
- 33   12. Habets RA, de Bock CE, Serneels L, et al. Safe targeting of T cell acute  
34   lymphoblastic leukemia by pathology-specific NOTCH inhibition. *Sci Transl Med.*  
35   2019;11(494).
- 36   13. Delgado-Martin C, Meyer LK, Huang BJ, et al. JAK/STAT pathway  
37   inhibition overcomes IL7-induced glucocorticoid resistance in a subset of human  
38   T-cell acute lymphoblastic leukemias. *Leukemia.* 2017;31(12):2568-2576.
- 39   14. Zhang J, Ding L, Holmfeldt L, et al. The genetic basis of early T-cell  
40   precursor acute lymphoblastic leukaemia. *Nature.* 2012;481(7380):157-163.
- 41   15. Ayala F, Dewar R, Kieran M, Kalluri R. Contribution of bone  
42   microenvironment to leukemogenesis and leukemia progression. *Leukemia.*  
43   2009;23(12):2233-2241.
- 44   16. Passaro D, Quang CT, Ghysdael J. Microenvironmental cues for T-cell  
45   acute lymphoblastic leukemia development. *Immunol Rev.* 2016;271(1):156-172.
- 46   17. Pitt LA, Tikhonova AN, Hu H, et al. CXCL12-Producing Vascular  
47   Endothelial Niches Control Acute T Cell Leukemia Maintenance. *Cancer Cell.*  
48   2015;27(6):755-768.

- 1 18. Passaro D, Irigoyen M, Catherinet C, et al. CXCR4 Is Required for  
2 Leukemia-Initiating Cell Activity in T Cell Acute Lymphoblastic Leukemia. *Cancer*  
3 *Cell.* 2015;27(6):769-779.
- 4 19. Duan CW, Shi J, Chen J, et al. Leukemia propagating cells rebuild an  
5 evolving niche in response to therapy. *Cancer Cell.* 2014;25(6):778-793.
- 6 20. Butler JM, Kobayashi H, Rafii S. Instructive role of the vascular niche in  
7 promoting tumour growth and tissue repair by angiocrine factors. *Nat Rev Cancer.*  
8 2010;10(2):138-146.
- 9 21. Nagl L, Horvath L, Pircher A, Wolf D. Tumor Endothelial Cells (TECs) as  
10 Potential Immune Directors of the Tumor Microenvironment - New Findings and  
11 Future Perspectives. *Front Cell Dev Biol.* 2020;8:766.
- 12 22. Jiang Y, Guo Y, Hao J, et al. Development of an arteriolar niche and self-  
13 renewal of breast cancer stem cells by lysophosphatidic acid/protein kinase D  
14 signaling. *Commun Biol.* 2021;4(1):780.
- 15 23. Vadillo E, Dorantes-Acosta E, Pelayo R, Schnoor M. T cell acute  
16 lymphoblastic leukemia (T-ALL): New insights into the cellular origins and  
17 infiltration mechanisms common and unique among hematologic malignancies.  
18 *Blood Rev.* 2018;32(1):36-51.
- 19 24. Sipkins DA, Wei X, Wu JW, et al. In vivo imaging of specialized bone  
20 marrow endothelial microdomains for tumour engraftment. *Nature.*  
21 2005;435(7044):969-973.
- 22 25. Cao Z, Scandura JM, Inghirami GG, Shido K, Ding BS, Rafii S. Molecular  
23 Checkpoint Decisions Made by Subverted Vascular Niche Transform Indolent  
24 Tumor Cells into Chemoresistant Cancer Stem Cells. *Cancer Cell.*  
25 2017;31(1):110-126.
- 26 26. McMillin DW, Negri JM, Mitsiades CS. The role of tumour-stromal  
27 interactions in modifying drug response: challenges and opportunities. *Nat Rev*  
28 *Drug Discov.* 2013;12(3):217-228.
- 29 27. Bakker E, Qattan M, Mutti L, Demonacos C, Krstic-Demonacos M. The role  
30 of microenvironment and immunity in drug response in leukemia. *Biochim Biophys*  
31 *Acta.* 2016;1863(3):414-426.
- 32 28. Habiel DM, Krepostman N, Lilly M, et al. Senescent stromal cell-induced  
33 divergence and therapeutic resistance in T cell acute lymphoblastic  
34 leukemia/lymphoma. *Oncotarget.* 2016;7(50):83514-83529.
- 35 29. Fahy L, Calvo J, Chabi S, et al. Hypoxia favors chemoresistance in T-ALL  
36 through an HIF1alpha-mediated mTORC1 inhibition loop. *Blood Adv.*  
37 2021;5(2):513-526.
- 38 30. Hopken UE, Rehm A. Targeting the Tumor Microenvironment of Leukemia  
39 and Lymphoma. *Trends Cancer.* 2019;5(6):351-364.
- 40 31. Sharma P, Hu-Lieskovan S, Wargo JA, Ribas A. Primary, Adaptive, and  
41 Acquired Resistance to Cancer Immunotherapy. *Cell.* 2017;168(4):707-723.
- 42 32. Seandel M, Butler JM, Kobayashi H, et al. Generation of a functional and  
43 durable vascular niche by the adenoviral E4ORF1 gene. *Proc Natl Acad Sci U S*  
44 *A.* 2008;105(49):19288-19293.
- 45 33. Cao Z, Ding BS, Guo P, et al. Angiocrine factors deployed by tumor  
46 vascular niche induce B cell lymphoma invasiveness and chemoresistance.  
47 *Cancer Cell.* 2014;25(3):350-365.

- 1 34. Townsend EC, Murakami MA, Christodoulou A, et al. The Public  
2 Repository of Xenografts Enables Discovery and Randomized Phase II-like Trials  
3 in Mice. *Cancer Cell*. 2016;29(4):574-586.
- 4 35. Qin H, Dong Z, Wang X, et al. CAR T cells targeting BAFF-R can  
5 overcome CD19 antigen loss in B cell malignancies. *Sci Transl Med*.  
6 2019;11(511).
- 7 36. Butler JM, Nolan DJ, Vertes EL, et al. Endothelial cells are essential for the  
8 self-renewal and repopulation of Notch-dependent hematopoietic stem cells. *Cell*  
9 *Stem Cell*. 2010;6(3):251-264.
- 10 37. Kobayashi H, Butler JM, O'Donnell R, et al. Angiocrine factors from Akt-  
11 activated endothelial cells balance self-renewal and differentiation of  
12 haematopoietic stem cells. *Nat Cell Biol*. 2010;12(11):1046-1056.
- 13 38. Laranjeira AB, de Vasconcellos JF, Sodek L, et al. IGFBP7 participates in  
14 the reciprocal interaction between acute lymphoblastic leukemia and BM stromal  
15 cells and in leukemia resistance to asparaginase. *Leukemia*. 2012;26(5):1001-  
16 1011.
- 17 39. Markovic A, MacKenzie KL, Lock RB. Induction of vascular endothelial  
18 growth factor secretion by childhood acute lymphoblastic leukemia cells via the  
19 FLT-3 signaling pathway. *Mol Cancer Ther*. 2012;11(1):183-193.
- 20 40. Teschendorff AE, Enver T. Single-cell entropy for accurate estimation of  
21 differentiation potency from a cell's transcriptome. *Nat Commun*. 2017;8:15599.
- 22 41. Lezon TR, Banavar JR, Cieplak M, Maritan A, Fedoroff NV. Using the  
23 principle of entropy maximization to infer genetic interaction networks from gene  
24 expression patterns. *Proc Natl Acad Sci U S A*. 2006;103(50):19033-19038.
- 25 42. Aifantis I, Raetz E, Buonamici S. Molecular pathogenesis of T-cell  
26 leukaemia and lymphoma. *Nat Rev Immunol*. 2008;8(5):380-390.
- 27 43. Van Vlierberghe P, Ferrando A. The molecular basis of T cell acute  
28 lymphoblastic leukemia. *J Clin Invest*. 2012;122(10):3398-3406.
- 29 44. Chen B, Tan Z, Gao J, et al. Hyperphosphorylation of ribosomal protein S6  
30 predicts unfavorable clinical survival in non-small cell lung cancer. *J Exp Clin*  
31 *Cancer Res*. 2015;34:126.
- 32 45. Pallis M, Harvey T, Russell N. Phenotypically Dormant and Immature  
33 Leukaemia Cells Display Increased Ribosomal Protein S6 Phosphorylation. *PLoS*  
34 *One*. 2016;11(3):e0151480.
- 35 46. Vlachos A. Acquired ribosomopathies in leukemia and solid tumors.  
36 *Hematology Am Soc Hematol Educ Program*. 2017;2017(1):716-719.
- 37 47. Zhang P, Lu Y, Gao S. High-mobility group box 2 promoted proliferation of  
38 cervical cancer cells by activating AKT signaling pathway. *J Cell Biochem*.  
39 2019;120(10):17345-17353.
- 40 48. Kwon JH, Kim J, Park JY, et al. Overexpression of high-mobility group box  
41 2 is associated with tumor aggressiveness and prognosis of hepatocellular  
42 carcinoma. *Clin Cancer Res*. 2010;16(22):5511-5521.
- 43 49. Qiu JJ, Lin XJ, Tang XY, Zheng TT, Lin YY, Hua KQ. Exosomal  
44 MetastasisAssociated Lung Adenocarcinoma Transcript 1 Promotes Angiogenesis  
45 and Predicts Poor Prognosis in Epithelial Ovarian Cancer. *Int J Biol Sci*.  
46 2018;14(14):1960-1973.

- 1 50. Gu Y, Jasti AC, Jansen M, Siefring JE. RhoH, a hematopoietic-specific Rho  
2 GTPase, regulates proliferation, survival, migration, and engraftment of  
3 hematopoietic progenitor cells. *Blood*. 2005;105(4):1467-1475.
- 4 51. Park JE, Botting RA, Dominguez Conde C, et al. A cell atlas of human  
5 thymic development defines T cell repertoire formation. *Science*. 2020;367(6480).
- 6 52. Le J, Park JE, Ha VL, et al. Single-Cell RNA-Seq Mapping of Human  
7 Thymopoiesis Reveals Lineage Specification Trajectories and a Commitment  
8 Spectrum in T Cell Development. *Immunity*. 2020;52(6):1105-1118 e1109.
- 9 53. D'Souza B, Meloty-Kapella L, Weinmaster G. Canonical and non-canonical  
10 Notch ligands. *Curr Top Dev Biol*. 2010;92:73-129.
- 11 54. Pietras A, von Stedingk K, Lindgren D, Pahlman S, Axelson H. JAG2  
12 induction in hypoxic tumor cells alters Notch signaling and enhances endothelial  
13 cell tube formation. *Mol Cancer Res*. 2011;9(5):626-636.
- 14 55. Tamura K, Hashimoto K, Suzuki K, Yoshie M, Kutsukake M, Sakurai T.  
15 Insulin-like growth factor binding protein-7 (IGFBP7) blocks vascular endothelial  
16 cell growth factor (VEGF)-induced angiogenesis in human vascular endothelial  
17 cells. *Eur J Pharmacol*. 2009;610(1-3):61-67.
- 18 56. Cheng SM, Chang YC, Liu CY, et al. YM155 down-regulates survivin and  
19 XIAP, modulates autophagy and induces autophagy-dependent DNA damage in  
20 breast cancer cells. *Br J Pharmacol*. 2015;172(1):214-234.
- 21 57. Dai Y, Chen S, Pei XY, et al. Interruption of the Ras/MEK/ERK signaling  
22 cascade enhances Chk1 inhibitor-induced DNA damage in vitro and in vivo in  
23 human multiple myeloma cells. *Blood*. 2008;112(6):2439-2449.
- 24 58. Zong CS, Chan J, Levy DE, Horvath C, Sadowski HB, Wang LH.  
25 Mechanism of STAT3 activation by insulin-like growth factor I receptor. *J Biol  
Chem*. 2000;275(20):15099-15105.
- 27 59. Waibel M, Vervoort SJ, Kong IY, et al. Epigenetic targeting of Notch1-  
28 driven transcription using the HDACi panobinostat is a potential therapy against T-  
29 cell acute lymphoblastic leukemia. *Leukemia*. 2018;32(1):237-241.
- 30 60. Bride KL, Vincent TL, Im SY, et al. Preclinical efficacy of daratumumab in  
31 T-cell acute lymphoblastic leukemia. *Blood*. 2018;131(9):995-999.
- 32 61. Mshaik R, Simonet J, Georgievski A, et al. HSP90 inhibitor NVP-BEP800  
33 affects stability of SRC kinases and growth of T-cell and B-cell acute  
34 lymphoblastic leukemias. *Blood Cancer J*. 2021;11(3):61.
- 35 62. Verbeke D, Gielen O, Jacobs K, et al. Ruxolitinib Synergizes With  
36 Dexamethasone for the Treatment of T-cell Acute Lymphoblastic Leukemia.  
37 *Hemasphere*. 2019;3(6):e310.
- 38 63. Frismantas V, Dobay MP, Rinaldi A, et al. Ex vivo drug response profiling  
39 detects recurrent sensitivity patterns in drug-resistant acute lymphoblastic  
40 leukemia. *Blood*. 2017;129(11):e26-e37.
- 41 64. Shi WY, Wang L, Xiao D, et al. Proteasome inhibitor bortezomib targeted  
42 tumor-endothelial cell interaction in T-cell leukemia/lymphoma. *Ann Hematol*.  
43 2011;90(1):53-58.
- 44 65. Indraccolo S, Minuzzo S, Masiero M, et al. Cross-talk between tumor and  
45 endothelial cells involving the Notch3-Dll4 interaction marks escape from tumor  
46 dormancy. *Cancer Res*. 2009;69(4):1314-1323.

- 1 66. Spiegel A, Kollet O, Peled A, et al. Unique SDF-1-induced activation of  
2 human precursor-B ALL cells as a result of altered CXCR4 expression and  
3 signaling. *Blood*. 2004;103(8):2900-2907.
- 4 67. Teicher BA, Fricker SP. CXCL12 (SDF-1)/CXCR4 pathway in cancer. *Clin  
5 Cancer Res*. 2010;16(11):2927-2931.
- 6 68. Schwartzman O, Savino AM, Gombert M, et al. Suppressors and activators  
7 of JAK-STAT signaling at diagnosis and relapse of acute lymphoblastic leukemia  
8 in Down syndrome. *Proc Natl Acad Sci U S A*. 2017;114(20):E4030-E4039.

9

**Figure 1**

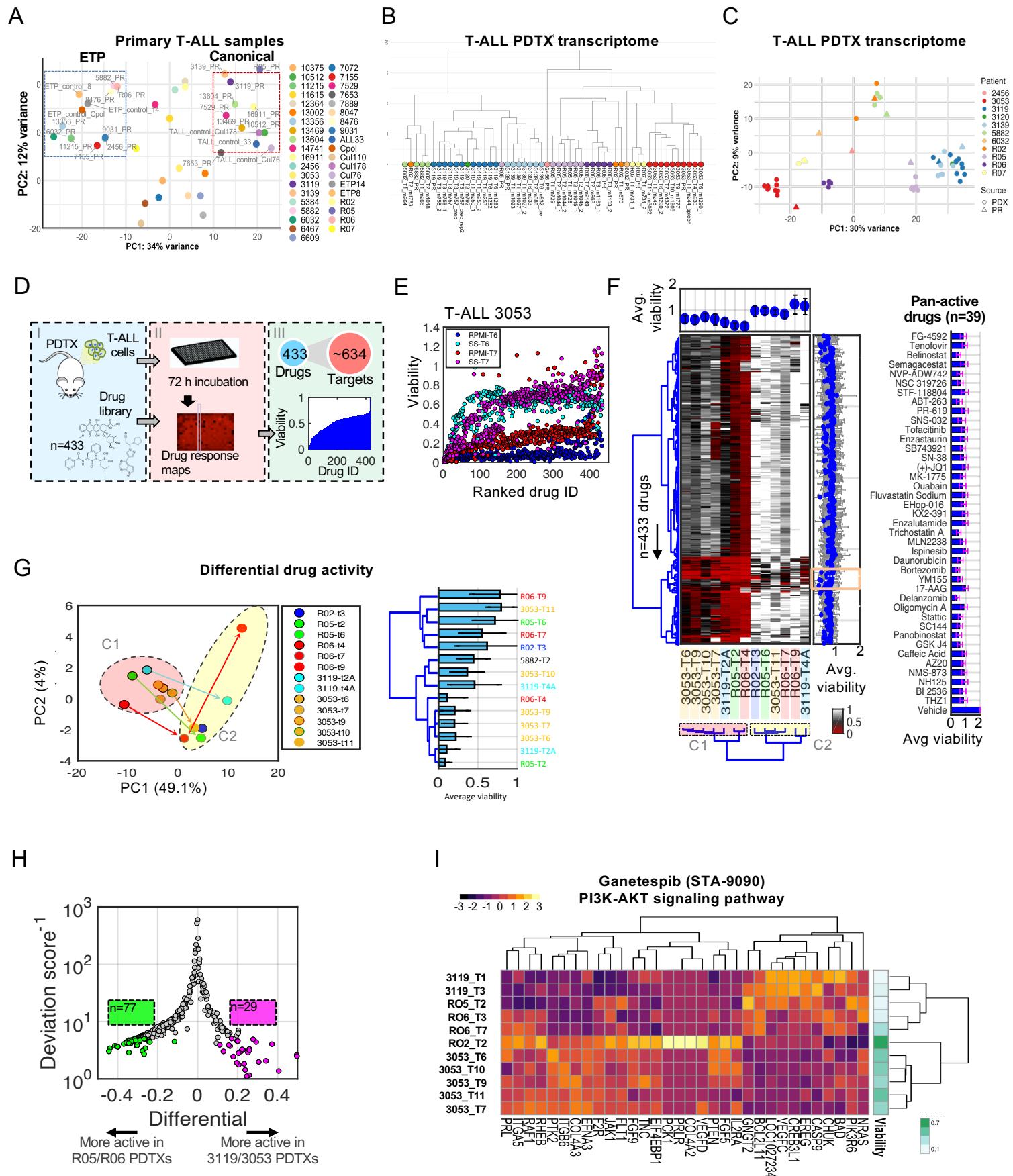


**Figure 2**

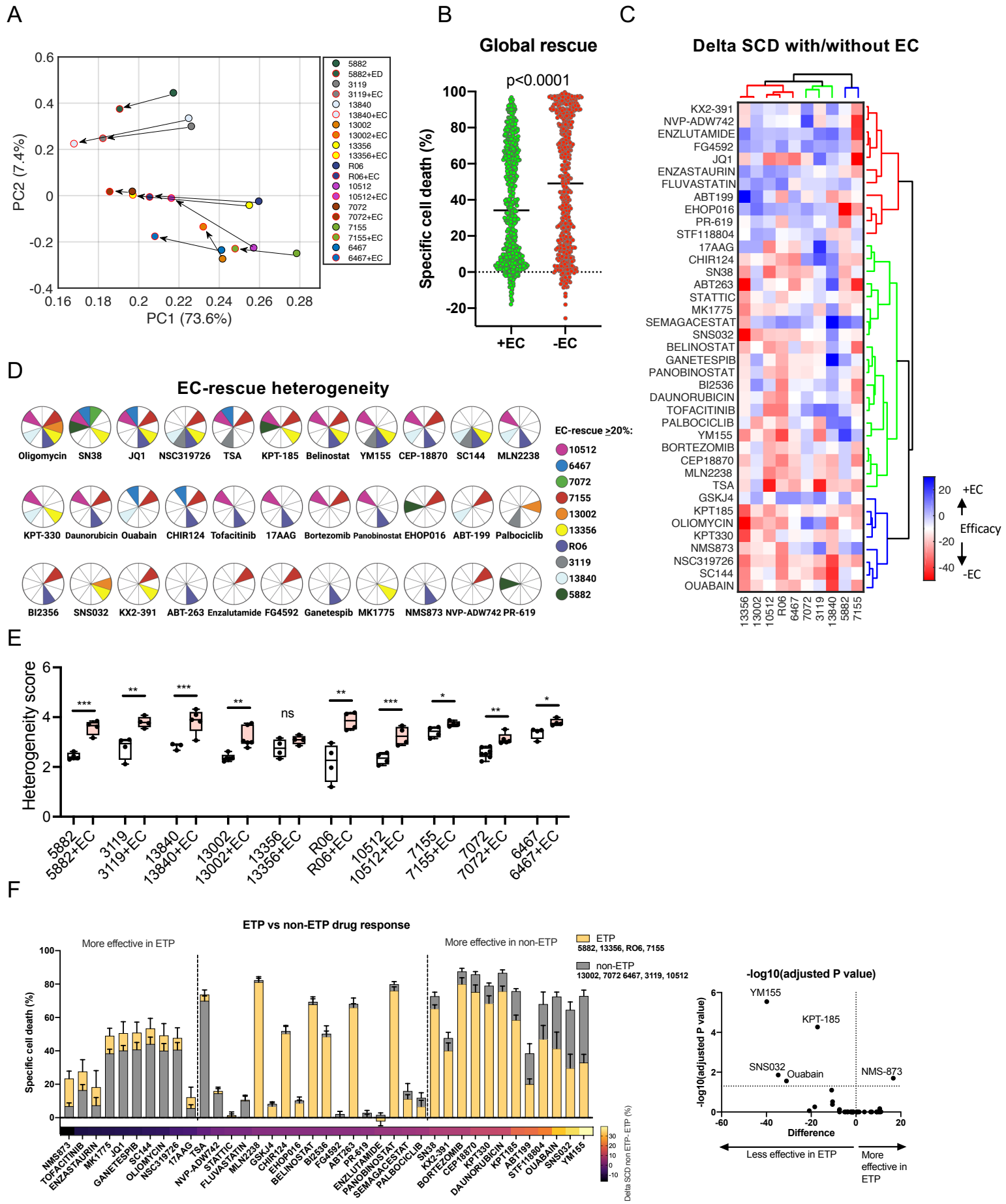
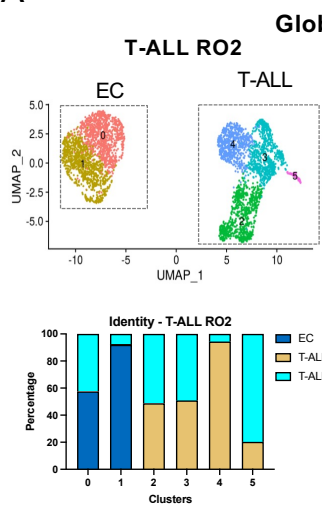
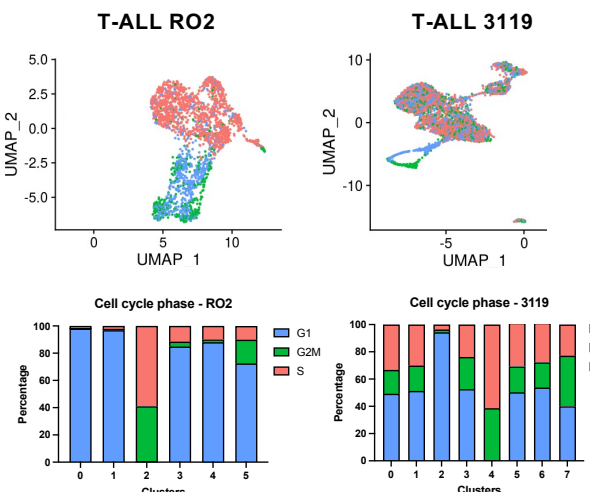


**Figure 3**

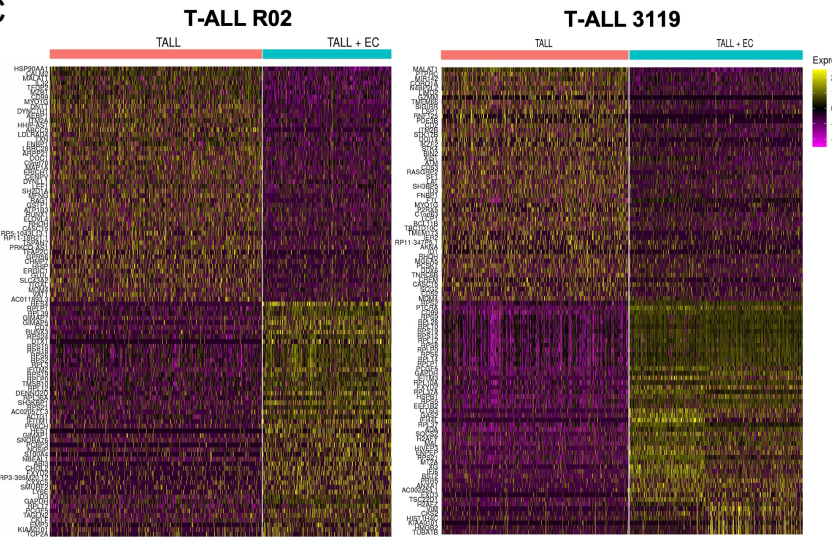
**A**



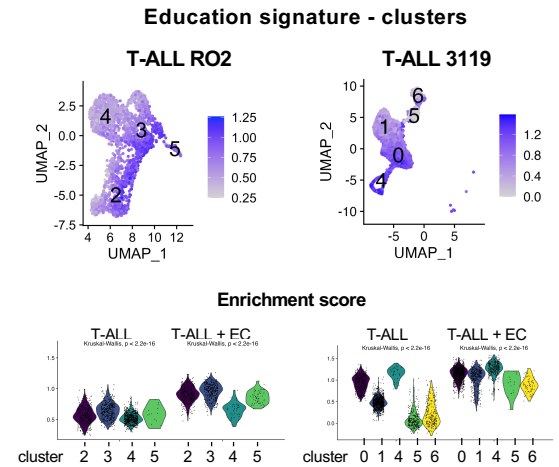
**B**



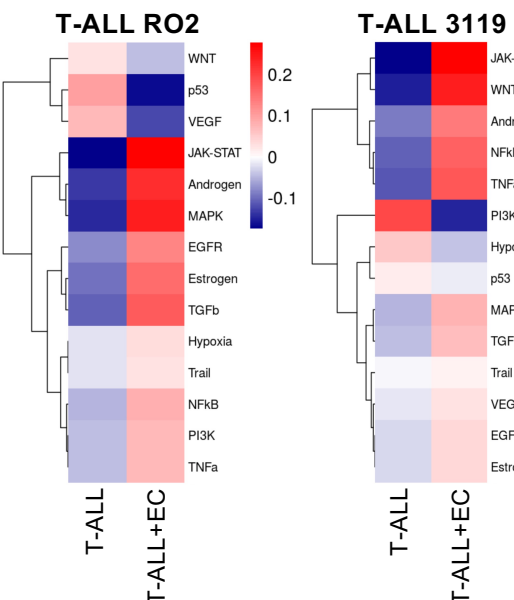
**C**



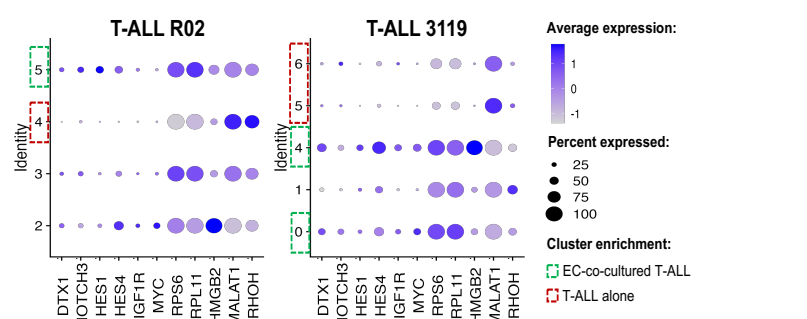
**D**



**E**



**F**



**G**

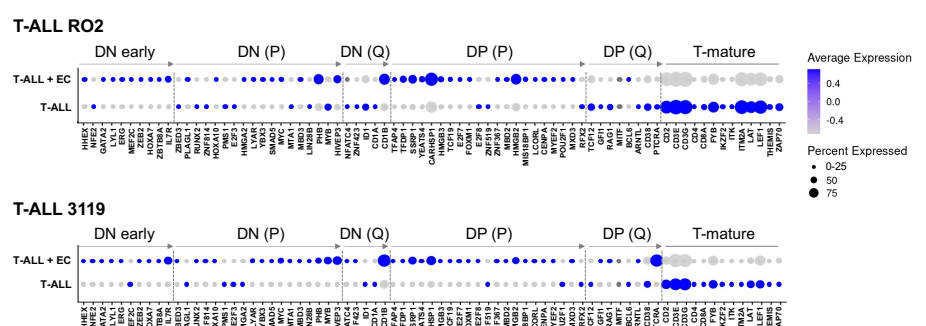


**Figure 4**

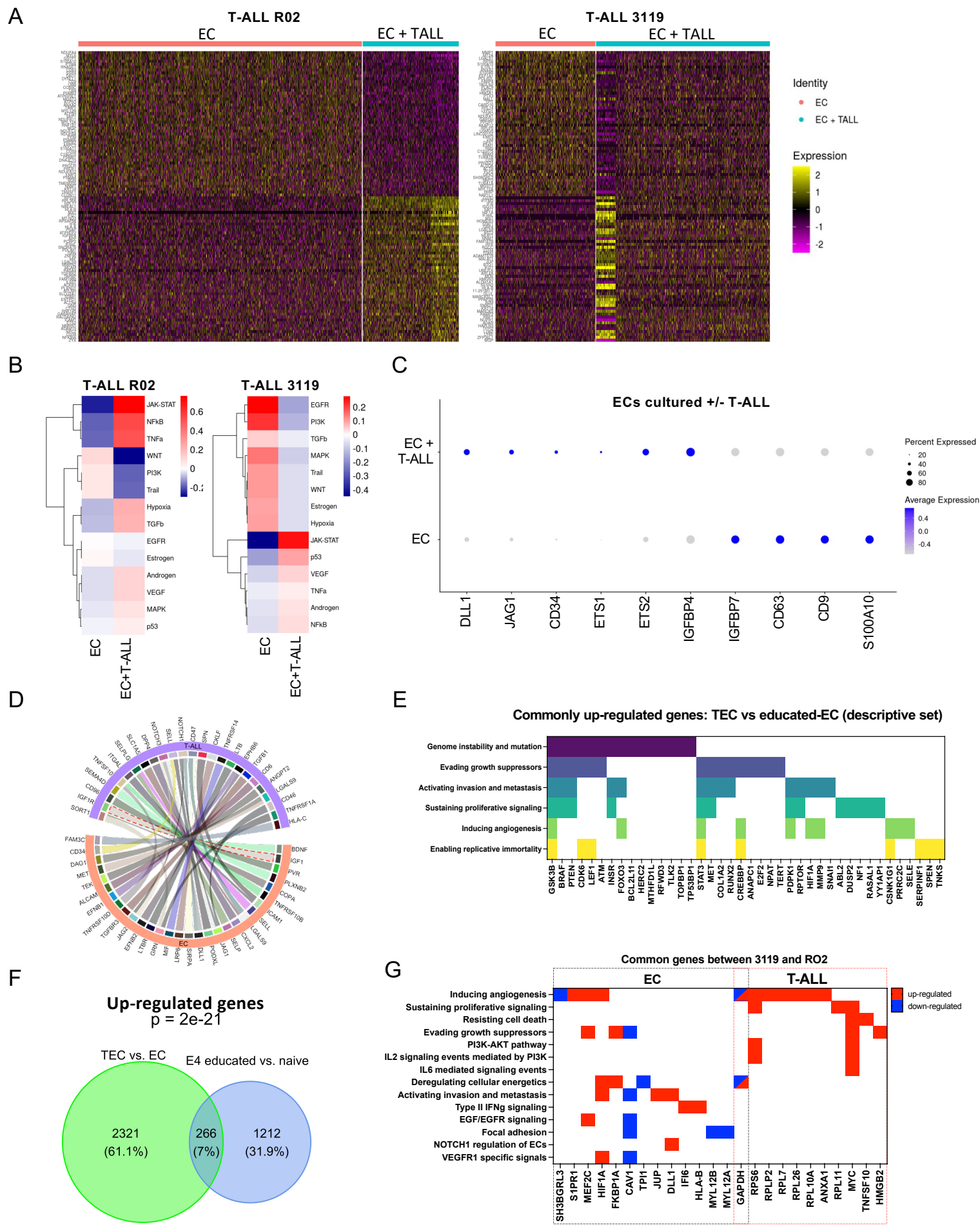
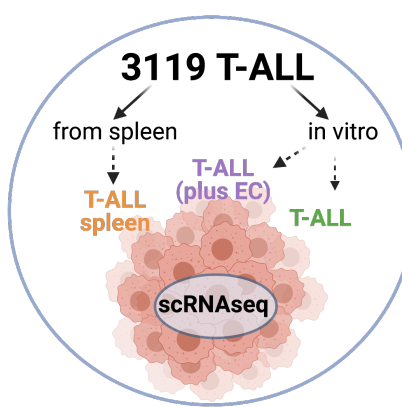
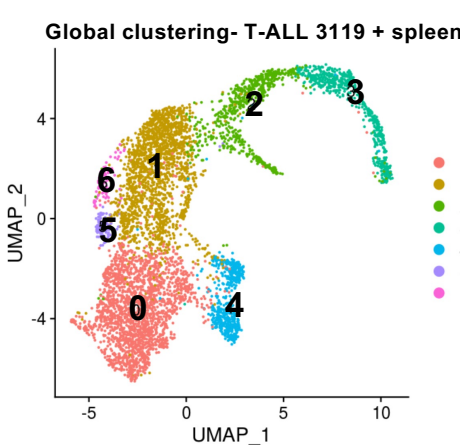


# Figure 5

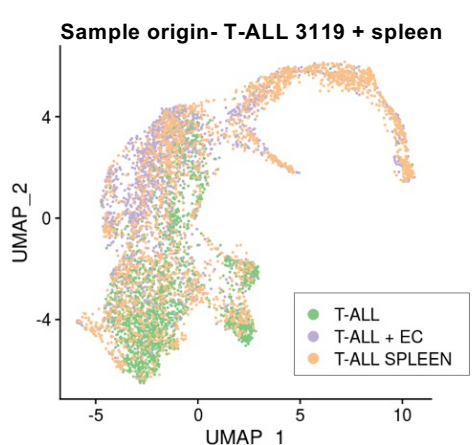
A



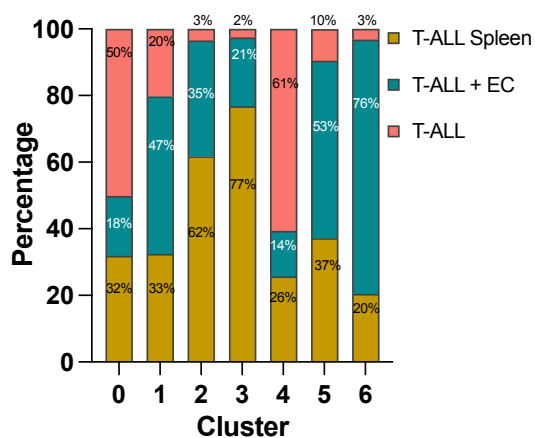
B



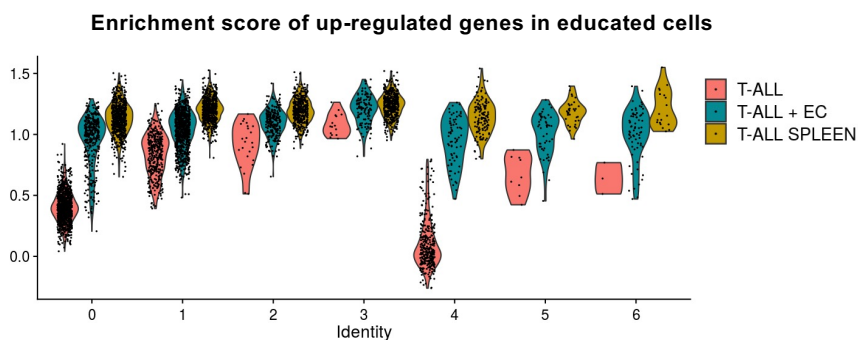
C



D



E



F

### Common T-ALL education signature genes in cluster 0

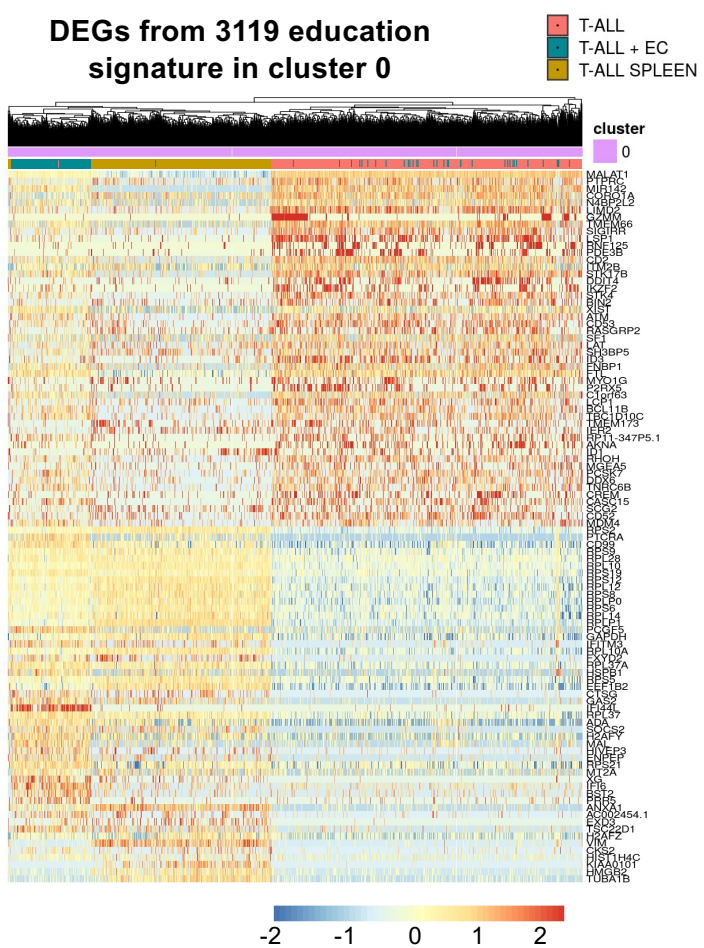
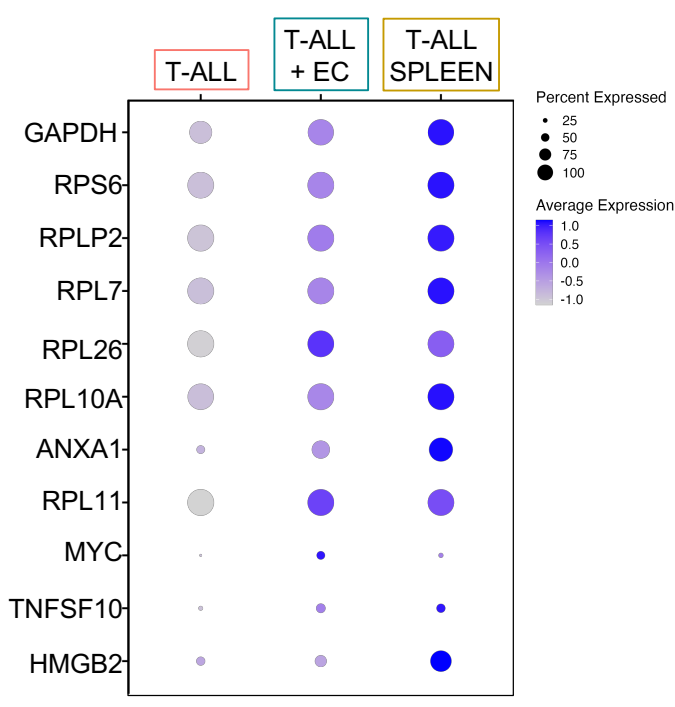
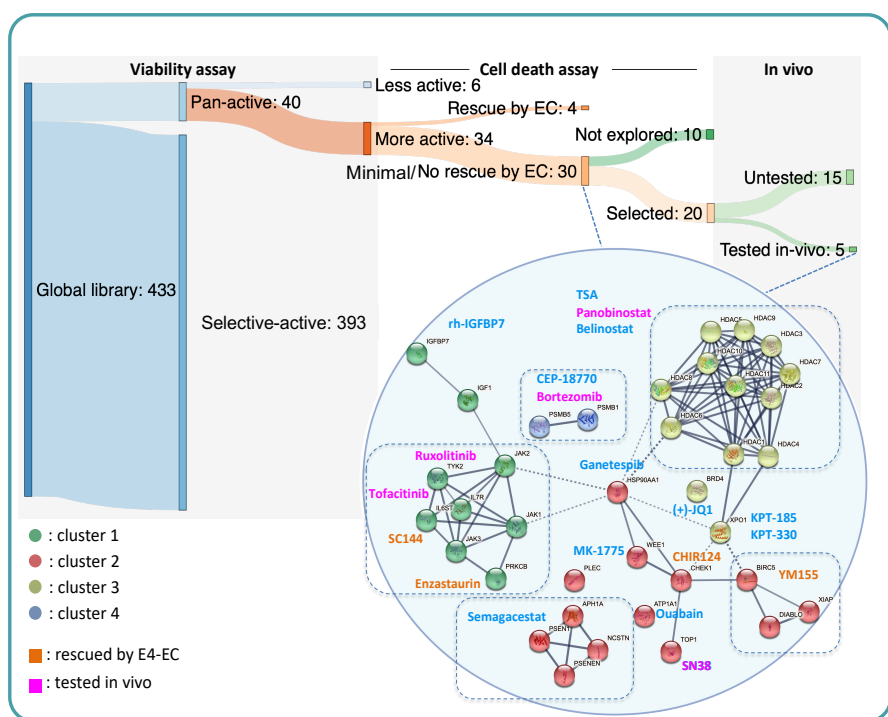
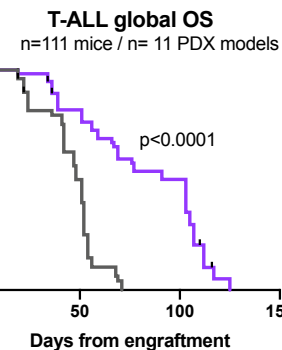


# Figure 6

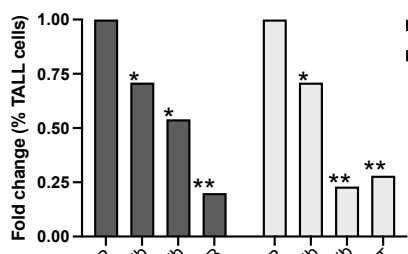
A



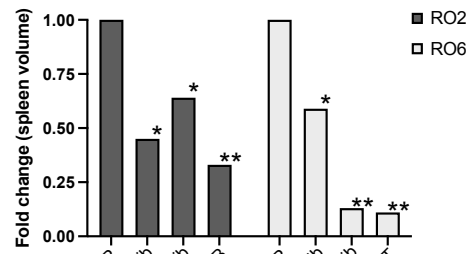
B



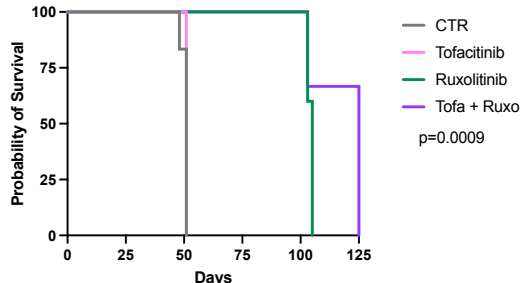
C



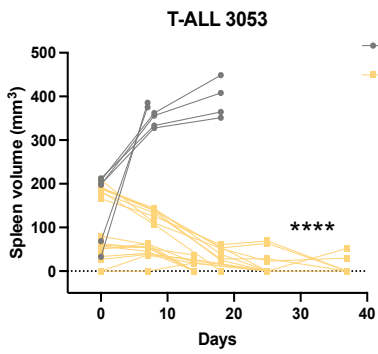
D



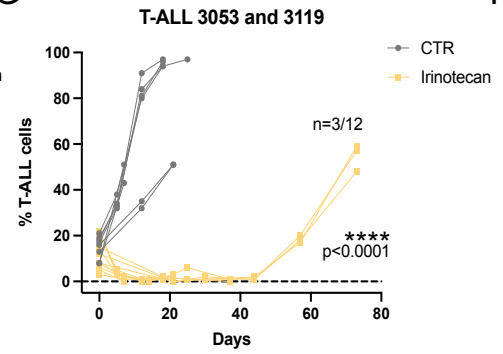
E



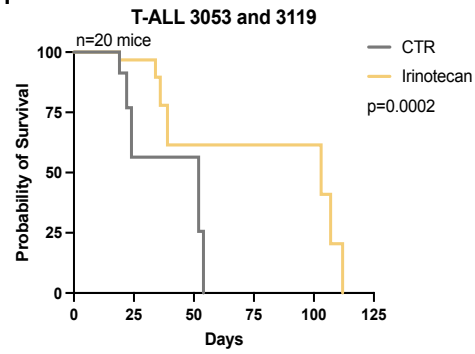
F



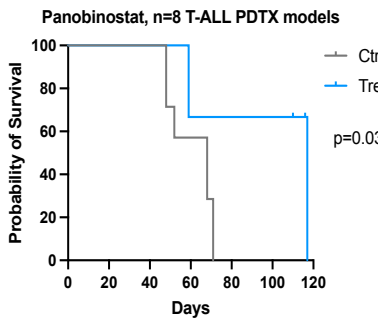
G



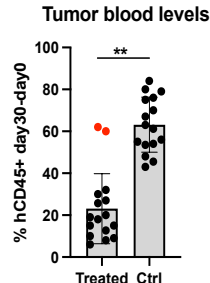
H



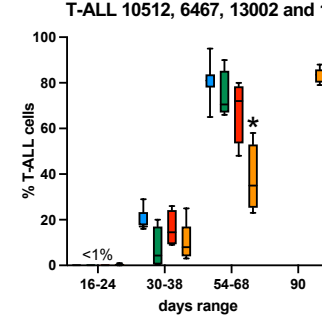
I



J



K



L

